



#### **OPEN ACCESS**

EDITED BY

Yaping Li, The Second Affiliated Hospital of Xi'an Jiaotong University, China

REVIEWED BY

Mohammed Rohaim. Cairo University, Egypt Mina Nakagawa, Tokyo Medical and Dental University, Japan

\*CORRESPONDENCE Omar A. Saldarriaga 

<sup>†</sup>These authors share first authorship

RECEIVED 08 July 2025 ACCEPTED 13 October 2025 PUBLISHED 10 November 2025

Millian DE, Arroyave E, Wanninger TG, Krishnan S. Bao D. Zhang JR. Rao A. Spratt H. Ferguson MR. Chen V. Henning K. Stevenson HL and Saldarriaga OA (2025) Exploring the liver microenvironment following successful therapy for HCV: gene expression profiling and residual T cell infiltration.

Front. Cell. Infect. Microbiol. 15:1662184. doi: 10.3389/fcimb.2025.1662184

© 2025 Millian, Arroyave, Wanninger, Krishnan, Bao, Zhang, Rao, Spratt, Ferguson, Chen. Henning, Stevenson and Saldarriaga. This is an open-access article distributed under the terms of the Creative Commons Attribution License (CC BY). The use, distribution or reproduction in other forums is permitted, provided the original author(s) and the copyright owner(s) are credited and that the original publication in this journal is cited, in accordance with accepted academic practice. No use distribution or reproduction is permitted which does not comply with these terms.

# Exploring the liver microenvironment following successful therapy for HCV: gene expression profiling and residual T cell infiltration

Daniel E. Millian<sup>1†</sup>, Esteban Arroyave<sup>1†</sup>, Timothy G. Wanninger<sup>2</sup>. Santhoshi Krishnan<sup>3,4</sup>, Daniel Bao<sup>5</sup>, Jared R. Zhang<sup>5</sup>, Arvind Rao<sup>3,4,6,7,8</sup>, Heidi Spratt<sup>9</sup>, Monique R. Ferguson<sup>10</sup>, Vincent Chen<sup>11</sup>, Kellen Henning<sup>2</sup>, Heather L. Stevenson<sup>1,5</sup> and Omar A. Saldarriaga 1\*

<sup>1</sup>Department of Pathology, University of Texas Medical Branch, Galveston, TX, United States, <sup>2</sup>Department of Microbiology and Immunology, University of Texas Medical Branch, Galveston, TX, United States, <sup>3</sup>Department of Computational Medicine and Bioinformatics, University of Michigan, Ann Arbor, MI, United States, <sup>4</sup>Department of Electrical and Computer Engineering, Rice University, Houston, TX, United States, 5John Sealy School of Medicine, University of Texas Medical Branch, Galveston, TX, United States, <sup>6</sup>Department of Radiation Oncology, University of Michigan, Ann Arbor, MI, United States, <sup>7</sup>Department of Biostatistics, University of Michigan, Ann Arbor, MI, United States, <sup>®</sup>Department of Biomedical Engineering, Rice University, Ann Arbor, MI, United States, <sup>9</sup>Department of Biostatistics and Data Science, University of Texas Medical Branch, Galveston, TX, United States, <sup>10</sup>Department of Internal Medicine, University of Texas Medical Branch, Galveston, TX, United States, <sup>11</sup>Department of Internal Medicine - Gastroenterology, University of Michigan, Ann Arbor, MI, United States

Background & aims: Direct-acting antivirals (DAAs) revolutionized hepatitis C (HCV) treatment. Yet, some patients present with persistent inflammation and still face adverse outcomes, including cirrhosis and hepatocellular carcinoma, despite achieving sustained virologic response (SVR).

Approach & results: This study examined liver biopsies from 22 patients before and after DAA treatment to assess gene and protein expression changes linked to disease progression. Pre-treatment, patients exhibited two distinct profiles: one characterized by high pro-inflammatory and antiviral gene expression (pre-hot), and another with weaker expression (pre-cold). Patients with pre-hot profiles were initially associated with poor outcomes (OR = 14.0, 95% CI: 1.31-178.5; p = 0.049), but this lost significance after adjusting for baseline disease severity (adjusted OR = 8.04, 95% CI: 0.18-2123.07; p = 0.328). Baseline modified hepatitis activity index (MHAI) scores (OR = 1.90, 95% CI: 0.72-6.34) and fibrosis stage (OR = 1.65, 95% CI: 0.44-9.97) trended toward predicting poor outcomes but were not significant. Post-treatment, liver enzymes decreased, inflammatory scores improved, and type I interferon pathways were restored, yet 14 of 17 patients (82.3%, 95% CI: 64.2-100%) retained persistent lymphocytic infiltrates. In parallel, spectral imaging further revealed post-treatment shifts in

macrophage populations, with a significant decrease in inflammatory subsets (CD14+, CD14+/Mac387+, p<0.05) and an increase in anti-inflammatory subsets (CD16+, CD16+/CD163+, CD16+/CD68+, p<0.05). Analysis of T cell-related marker expression before and after treatment shows that mixed lymphocytic infiltration (CD3+, CD4+, CD8+, CD45RO+) persists within the liver despite viral clearance, with high inter-patient variability likely limiting statistical significance. **Conclusions:** Even after achieving SVR and normalization of gene expression, the liver retained a heterogeneous T cell infiltrate, suggesting that persistent immune activity could continue to influence the risk of adverse outcomes.

KEYWORDS

hepatitis C virus, direct-acting antiviral, sustained virologic response, liver, hepatic microenvironment

# Introduction

Although hepatitis C virus (HCV) infection continues to be a global health challenge, with approximately 50 million infected globally and one million new cases each year, the landscape has shifted dramatically in recent years due to the availability of directacting antiviral (DAA) therapy (Burki, 2024). By selectively targeting enzymes essential for viral replication, DAAs have achieved cure rates higher than 90% (Oru et al., 2021). This has substantially reduced the number of patients progressing to chronic HCV, the occurrence and recurrence of hepatocellular carcinoma (HCC), and all-cause mortality, which represent significant milestones in the clinical management of patients infected with HCV (Mendizabal et al., 2020). However, despite many patients achieving sustained virologic response (SVR) after DAA treatment, many individuals in high-risk populations remain susceptible to reinfection due to the absence of an effective vaccine and the surge in HCV incidence driven by the opioid epidemic. Specifically, injection drug users account for approximately 70% of new HCV infections (Ko et al., 2019).

The liver is a unique immune organ enriched with a diverse array of myeloid and lymphoid cells, and it relies on tolerogenic mechanisms to maintain homeostasis. HCV infection disrupts this balance by triggering the activation of both innate (e.g., type I interferons and IFN-stimulated genes) and adaptive immune responses (e.g., helper and cytotoxic T cells), which play a crucial role in either mediating viral clearance or sustaining chronicity (Noureddin et al., 2015). Inflammatory macrophage activation and cytotoxic T cell responses are typically protective, as they help to control viral replication and eliminate infected cells. However, the impairment of inflammatory macrophages and T cells, the induction of alternatively activated macrophages involved in tissue repair processes, and the promotion of exhausted T cells (characterized by a loss of effector functions and sustained

expression of inhibitory receptors) contribute to HCV persistence in the liver (Saha et al., 2016; Ahmed et al., 2019; Barili et al., 2020). Human immunodeficiency virus (HIV) coinfection exacerbates HCV-induced inflammation and impairs both the innate and adaptive immune responses against HCV (Abutaleb and Sherman, 2018). DAAs have shown the potential to reverse these mechanisms and boost anti-HCV immunity.

In some cases, patients treated with DAAs exhibit persistent inflammation in the portal tracts of the liver without changes in the fibrosis stage or features of regression (Hsieh et al., 2021). Posttreatment lymphocytic inflammation, distinguished from other types of active hepatitis by its confinement to the portal tracts without interface and lobular activity, can still pose a diagnostic challenge for clinicians and pathologists managing HCV patients (Saldarriaga et al., 2021). Persistent lymphocytic portal inflammation is frequently observed in allograft liver biopsies after treatment, which can be puzzling and create uncertainty about whether the virus has truly been eliminated, despite clinical evidence of SVR (Whitcomb et al., 2017). Moreover, it is unclear whether patients who achieve SVR but exhibit histological evidence of persistent lymphocytic inflammation are predisposed to adverse outcomes, such as cirrhosis or cancer. Advanced imaging and single-cell platforms have been used to enhance understanding of changes in both the cellular composition and spatial distribution within the hepatic microenvironment (MacParland et al., 2018). However, studies of the liver after DAA treatment in the absence of HCV are limited, in part because the current standard of care no longer includes pre- or post-treatment liver biopsies, thereby reducing the availability of tissue for analysis (Bhattacharya et al., 2023).

This study aimed to analyze gene and protein expression changes in the hepatic microenvironment of patients before and after DAA treatment for HCV. It is unique in its access to liver biopsies from patients' post-treatment, a resource that is rarely

available under current clinical practice. This allowed us to correlate individual gene and protein signatures detected in the hepatic microenvironment with clinical outcomes and disease progression.

blocks were stored at room temperature and sectioned before staining; unstained slides were stored at -80 °C when necessary.

### Materials and methods

# Study design and patient inclusion criteria

We evaluated liver biopsies collected from adult patients before (i.e., pre-treatment) and after (i.e., post-treatment) DAA therapy for HCV, at the University of Texas Medical Branch (UTMB), between January 2008 and June 2021. This study was approved by the UTMB Institutional Review Board (IRB#13-0511), and all patients provided informed consent for research use of their tissue samples. The first biopsy was collected for diagnostic purposes prior to DAA treatment, while post-treatment biopsies were obtained only from patients who consented, as biopsy is not standard of care after SVR. The cohort included 22 patients: Seventeen patients with paired pre- and post-treatment biopsies, five with only pre-treatment biopsies, and one with only a post-treatment biopsy. Samples (pre and post) were matched by patient identifiers to allow longitudinal comparison. Demographic data, HCV viral load, and laboratory tests were recorded for all patients. No participants under 18 met the inclusion criteria.

# Control group criteria

Controls were individuals without liver disease, selected to provide a healthy baseline for gene expression profiling. They had no history of HCV or other hepatotropic infections, HIV, excessive alcohol/substance use, metastatic liver cancer, or immune-mediated liver conditions. Their biopsies showed no histopathologic abnormalities and liver enzymes were within normal ranges; however, control patients were not matched (Supplementary Table S1).

# Biopsy collection and histological assessment

Liver biopsies were obtained as part of standard care by licensed radiologists and processed in a College of American Pathologists (CAP)-accredited laboratory as described previously (Saldarriaga et al., 2021) and evaluated by a board-certified liver pathologist (H.S.L) blinded to the patient's serology and clinical history. Histologic features were scored using the modified hepatitis activity index (MHAI) for inflammatory activity, Ishak staging for fibrosis, and steatosis grading (Ishak et al., 1995). Digital images were acquired using an Aperio ImageScope scanner. Adverse clinical outcomes, including HCC, were diagnosed based on standard clinical practice, typically using imaging modalities, in line with established guidelines. MELD scores were used to assess overall liver disease severity, not to confirm HCC diagnosis. Tissue

# DAA treatment regimen and response to therapy

Patients received DAA regimens according to international guidelines for up to 12 weeks. Only those who achieved SVR were included. No patients had serologic evidence of coinfection with other hepatotropic viruses (e.g., hepatitis A, B, or E) or immunemediated liver disease at diagnosis or during the study.

# Laboratory tests

Pre- and post-treatment laboratory tests (alanine aminotransferase [ALT], aspartate aminotransferase [AST], alkaline phosphatase [ALP], albumin, bilirubin, platelets, prothrombin time [PT], and international normalized ratio [INR]) were performed for all 22 patients. Viral load, genotype, and liver enzyme levels were assessed using CAP- and Clinical Laboratory Improvement Amendments (CLIA)-accredited molecular tests at baseline, three to four months after DAA treatment, and during follow-up.

# RNA isolation and nCounter gene expression analysis

RNA was extracted from formalin-fixed, paraffin-embedded (FFPE) and fresh liver biopsies, ensuring strict quality criteria (DV300 > 50%,  $260/280 \ge 1.7$ ). Gene expression profiling was performed by hybridizing 50–150 ng of RNA with the PanCancer Immune Panel (730 immunological, inflammatory, and anti-viral targets and 40 housekeeping genes) on the nCounter platform (NanoString, Bruker Spatial Biology, Seattle, WA, USA). Quality control, normalization, differential expression, and immune-related scoring were conducted using nSolver  $4.0^{\rm TM}$  analysis software. Normalization was performed using the most stable housekeeping genes, identified by the geNorm algorithm based on pairwise variation analysis (26 of the 40 available housekeeping genes were retained)(Supplementary Table S2).

# Differential gene expression and bioinformatics analysis

Hierarchical clustering, principal component analysis (PCA), volcano plots, and Venn diagrams were used to compare gene expressions among HCV pre- and post-DAA groups and controls. Differential expression analysis was performed using nSolver (NanoString/Bruker), which models counts data using a negative binomial model (glm.nb function) and applies Wald tests for group comparisons. Fold changes were calculated as log2 ratios between groups, and p-values were adjusted for multiple comparisons using

the Benjamini-Yekutieli (B-Y) method. Volcano plots were generated by plotting log2 fold change on the x-axis against -log10 adjusted p-value on the y-axis. Significance thresholds were defined as B-Y FDR < 0.05 with log2 fold change  $\geq \pm 0.6$ . PCA was performed on log2-transformed, mean-centered, and unit-variance scaled gene expression data. The percentage of variance explained by each principal component was calculated and is indicated on the PCA plots. Volcano plots and PCA were visualized using GraphPad Prism v.10 (GraphPad Software, San Diego, CA, USA). Functional enrichment analysis was performed using the Database for Annotation, Visualization, and Integrated Discovery (DAVID) tool with Reactome database integration. Immune cell composition was estimated using CIBERSORTx, which infers relative cell-type proportions by comparing expression data against the LM22 reference matrix (547 RNAseq-derived genes). Analyses were run with 500 permutations and B-mode batch correction to enhance robustness. Normalized NanoString PanCancer Immune Panel data (730 genes) were deconvolved against LM22 using overlapping genes between the two platforms. In total, 181 genes overlapped, including canonical markers for major T-cell subsets and macrophage/monocyte lineages (Chen et al., 2018). This overlap ensured adequate immune-specific coverage, enabling reliable estimation of the targeted populations in this study.

# Multispectral imaging analysis

Two multiplex antibody panels were used, targeting macrophages (CD68, CD163, Mac387, CD14, CD16) and T cells (CD3, CD4, CD8, CD45RO, FoxP3) with DAPI counterstaining. Staining was conducted manually, or with the Ventana discoveryultra (Roche Diagnostics, Indianapolis, IN), under the conditions detailed in Supplementary Tables S3, S4, as previously described. Tissue sections were imaged using the Vectra 3 quantitative pathology imaging system (Akoya Biosciences, Marlborough, MA) at 20× magnification, with exposure settings optimized for each Opal fluorophore to avoid signal saturation (e.g., Opal 520, 540, 570, 620, 650, 690). Regions of interest (ROIs) were acquired from at least 50% of the tissue area for macrophage panel and from approximately 100% for the T cell panel, corresponding to 30-60 images per liver biopsy and ensuring substantial tissue representation. Imaging was performed using stamped acquisition areas of 2  $\times$  2 (1,338  $\mu$ m  $\times$  1,000  $\mu$ m) at a resolution of 0.5  $\mu$ m (20 $\times$ ) (Saldarriaga et al., 2024). ROIs included both portal tracts and lobular regions, and no additional tissue segmentation was applied. Images and ROIs were selected using automated detection and processed with inForm software (Akoya Biosciences, Marlborough, MA), to generate multi-component TIFF files, which were subsequently analyzed in Visiopharm (Hoersholm, Denmark) using deep learning-based AI algorithms for tissue and nuclear identification, and cell phenotype classification. Nuclei were detected based on DAPI staining using a segmentation procedure that includes a trained neural network algorithm as well as size and shape thresholds to separate overlapping nuclei (typical size range  $5\text{--}20~\mu\text{m}^2$ ). Fluorescent markers were quantified in the corresponding channels within nuclear (e.g., Mac387) or cytoplasmic (e.g., CD163) masks, and cells were classified based on intensity thresholds or machine-learning classifiers trained on representative ROIs. To compare marker expression across patients, cell counts were quantified as the proportion of marker-positive cells relative to the total cell population (DAPI +). Inter- and intrarun reproducibility were managed using a semi-automated staining protocol combined with optimized AI algorithms for quantification, which were validated for each patient sample prior to automated analysis. AI-assisted analysis provides automated, reproducible cell-type quantification within automatically selected ROIs, validated through expert review.

# Statistical analysis

Histological, laboratory data and gene expression analyses were conducted in R (v4.4.3) using the limma package (v3.62.2). Prior to differential expression analysis, we assessed the relationship between RNA quality and sample storage characteristics. A multiple linear regression model was employed to evaluate the impact of storage duration (in years) and storage type (FFPE vs. fresh frozen) on RNA quality using the lm function in R. The storage type was identified as a confounder ( $\beta = 69.28$ , SE = 16.62, p < 0.001) and incorporated as a covariate in the limma design matrix. To further account for both paired and unpaired samples across control, pre, and post groups, within-patient correlations were estimated using duplicateCorrelation. Linear models were then fit with lmFit (block = patient\_id) incorporating the consensus correlation, followed by empirical Bayes moderation (eBayes) to stabilize variance estimates. Pairwise contrasts (pre vs control, post vs control, post vs pre) were specified with makeContrasts, and moderated t-statistics and raw p-values were calculated. P-values were adjusted for multiple testing using the Benjamini-Hochberg (B-H) procedure to control the false discovery rate (FDR), allowing inclusion of all samples while accounting for repeated measures. Normality of the cell marker data and other variables was assessed using the Shapiro-Wilk test. Depending on the comparison, paired or unpaired t-tests were applied as appropriate. To account for multiple comparisons (macrophages and T cells phenotypes), raw p-values were adjusted using the Bonferroni method in R, yielding the final adjusted p-values. Associations between pre-DAA gene expression and clinical outcomes were determined using Fisher's exact test, with odds ratios (OR) >1 indicating positive associations. To assess potential confounding variables affecting outcomes (poor vs. good), we performed multivariable logistic regression in R, adjusting for baseline fibrosis stage, MHAI scores, and HIV status. Boxplots, volcano plots, PCAs, and heatmaps were generated using GraphPad Prism v10.3.0 (GraphPad Software, San Diego, CA, USA).

# Results

# Study design

This study aimed to analyze gene and protein expression changes in pre- and post-DAA treatment to assess immune responses following HCV clearance. Gene and protein signatures were also correlated with inflammatory activity, fibrosis stages, and clinical outcomes. We previously correlated the light microscopy findings with clinical outcomes in 10 patients (Saldarriaga et al., 2021). Here, we expanded the cohort to 22 patients, analyzing nCounter gene expression and multispectral imaging in parallel patient subsets with partial overlap, to evaluate hepatic immune dynamics over time. The experimental workflow is shown in Figure 1A. Liver biopsies were collected pre- and post-DAA treatment. RNA from Study Patient Set 1 underwent NanoString nCounter gene expression analysis. Unstained biopsy sections from Study Patient Set 2 were stained with a macrophage panel, whereas slides from Study Patient Set 3 were stained with a T cell panel, acquired with multispectral imaging, and analyzed using Visiopharm. Patients analyzed in the different experiments partially overlap, with some included in both gene expression and macrophage or T cell panels (Table 1; Figure 1A).

# Demographics and clinical data

Patient demographics, histological scoring, and clinical data, including viral loads and genotypes, are shown in Table 1. The cohort included 14 males and eight females, with a mean age of  $52.45 \pm 6.58$  years at first biopsy and  $54.82 \pm 7.82$  years posttreatment. Patients were predominantly White (64.29%) and non-Hispanic (77.0%). Body mass index (BMI) remained stable from baseline to post-treatment (28.22  $\pm$  6.09 kg/m<sup>2</sup> to 29.70  $\pm$  6.97 kg/  $m^2$ , p = 0.52 (Supplementary Table S1; Table 1). The control group included eight males and seven females (mean age: 53.8 ± 12.9 years). Race distribution was 80.0% White and 20.0% non-White, and ethnicity distribution was 20% Hispanic and 80% non-Hispanic. Although controls, were not matched to study patients, no significant differences in age, sex, race, ethnicity, or BMI were observed when compared with the pre-DAA group (Supplementary Table S1). The most prevalent genotype in the pre-DAA treatment group was 1a (55%), followed by 1b (18%) and 2b (18%) (Table 1). After treatment, inflammatory activity (MHAI) decreased significantly from 4.81  $\pm$  2.10 to 2.40  $\pm$  1.14, along with AST (67  $\pm$  74 U/L to 28  $\pm$  11.56 U/L) and ALT (74  $\pm$  79.64 U/L to 28  $\pm$  11.6 U/L) (p < 0.001). Fibrosis stage and major liver function and coagulation markers (ALP, PT, albumin, total bilirubin, platelets, INR) showed no significant change (Figure 1B).

# Gene expressions change pre- and post-DAA treatment

Unsupervised Hierarchical clustering of gene expression data (Figure 2A) revealed two distinct clusters: one with low ("cold") overall gene expression profile [controls (eight out of eight), most

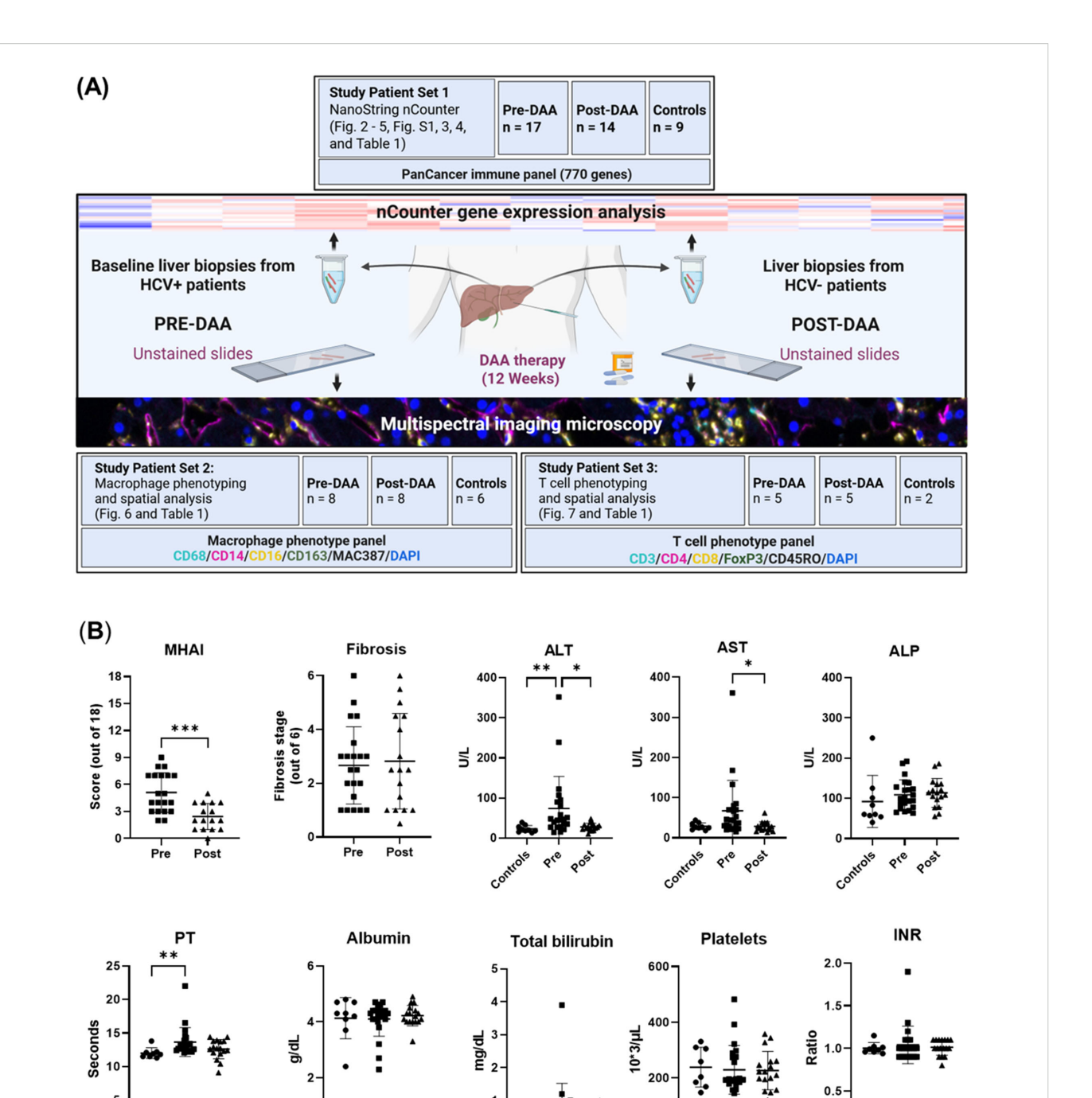
post-DAA (eleven out of fourteen), half pre-DAA (eight out of seventeen)] and another with high ("hot") gene expression profile [half pre-DAA (nine out of seventeen), a few post-DAA (three out of fourteen)]. Principal component analysis (PCA, Figure 2B), using all genes, confirmed the same separation, with cluster assignments from Figure 2A used to outline groups. The reproducibility of the clustering was supported by the consistent identification of the same two groups using both hierarchical clustering and PCA.

Compared to controls, pre-DAA treatment patients exhibited upregulation of inflammatory and antiviral genes (STAT2, CXCL10, CXCL9, IFNAR2, ISG15, OAS3, MX1, IFI27, IFI35), highlighting an active immune response to chronic HCV infection. These expression levels declined post-DAA treatment, aligning with controls and indicating resolution of the antiviral immune response (Figure 2C; Supplementary Tables S5, S6), consistent with previous reports (Boldanova et al., 2017). Pathway analysis revealed the enrichment of immune-related and host-virus interaction pathways pre-DAA, with a significant decrease observed post-DAA, returning to levels comparable to controls (Figures 2D, E). Inflammatory (CXCL10, STAT1) and interferoninduced antiviral genes (MX1, OAS3, ISG15, ISG20, IFI27, IFI35, IFIT1, IFIT2) were significantly downregulated post-DAA (p < 0.05), consistent with the resolution of the antiviral immune response as previously reported (Burchill et al., 2021). Marked heterogeneity was observed in log2 expression levels across patients pre- and post-DAA (Figure 2E).

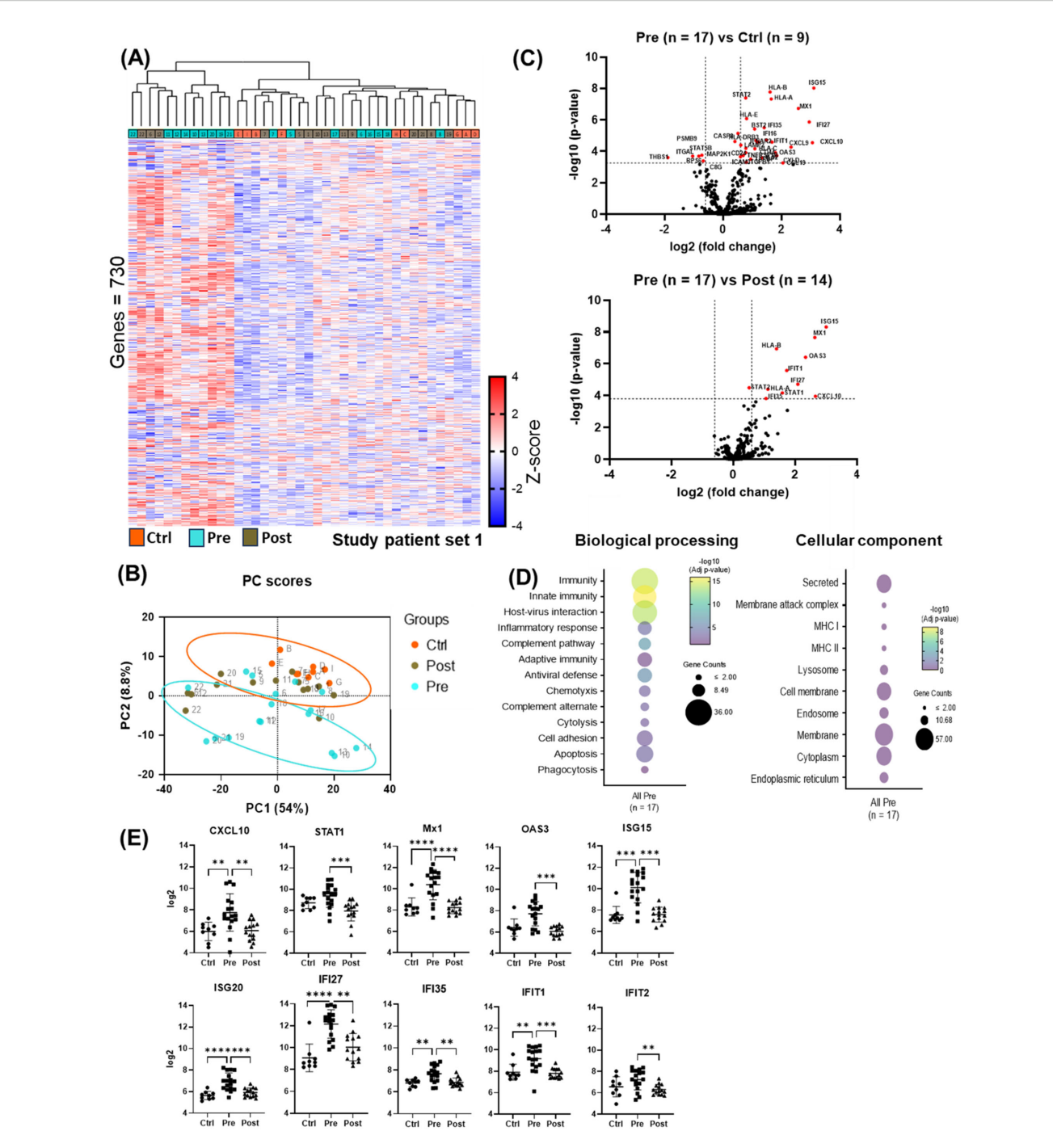
Cell deconvolution analysis revealed that, among the immune cells shaping the liver landscape in the patient groups, M1 macrophages were elevated pre-treatment (p < 0.05) but declined significantly post-DAA (p < 0.01), consistent with reduced hepatic inflammation. T cells showed a trend toward increased gene expression pre-DAA compared to controls, with CD8+ T cells showing a significant (p<0.05) increase pre-DAA that remained unchanged post-DAA (Figures 3A, B). Unexpectedly, CD14 and CD16 gene expression were highest in controls, with no significant differences between pre- and post-treatment groups (Figure 3C). Notably, CD4 expression was significantly higher in the controls compared to pre- and post-treatment groups, while CD8A a marker of cytotoxic CD8+ T cells, was upregulated (p<0.05) in the pre-DAA group compared to controls (Figure 3D; Supplementary Figure S1). These gene expression findings motivated a complementary analysis of protein expression in a separate subset of patients (see multispectral imaging section).

# Gene expression revealed distinct subclusters in HCV patients pre- and post-DAA

Within the pre-DAA group, two subgroups emerged: pre-hot (high inflammatory gene expression, n = 9) and pre-cold (low gene expression, n = 8) (Figure 2A). Pre-hot patients exhibited increased inflammatory (CXCR4, BCL2, FYN, NLRC5, LTB, CCL3, IKBKE, IRF7, JAK3, TNFAIP3, CXCL9) and cancer progression gene markers (i.e., CXCR4, BCL2, FYN) (Lin et al., 2014; Hosseini-Khah et al., 2021;



Experimental workflow and comparison of clinical data of patients pre- and post-DAA treatment for viral hepatitis C. (A) This study evaluated differences in the hepatic microenvironment of liver biopsies collected from patients with HCV (n = 22: 16 patients had paired pre-and post-treatment biopsies, five had only pre-treatment biopsies, and one had only a post-treatment biopsy, see also Table 1) and controls (n = 15; two controls used for T cell phenotyping were also used for macrophage phenotyping analysis) using gene expression and spectral imaging (see also Supplementary Table S1). Post-treatment biopsies were collected after SVR. RNA was extracted from fresh liver and FFPE slides for nCounter analysis (Set 1). Spectral imaging was performed on pre- and post-DAA biopsies using macrophage (Set 2) and T cell (Set 3) panels. Multicomponent TIFFs were imported into the Visiopharm digital software platform to generate phenotype profile maps. (B) Clinical comparison of patients pre- and post-DAA, and controls. Post-DAA patients showed significantly reduced inflammatory activity (MHAI score) and lower ALT/AST levels. Liver biopsies were graded for inflammatory activity using the MHAI scoring criteria (0-18) and staged for fibrosis using Ishak (1-6) criteria. Histological and laboratory data were analyzed using limma (R/Bioconductor), accounting for paired (pre/post) and unpaired samples with duplicateCorrelation function; linear models with empirical Bayes moderation were used, and p-values were adjusted by the B-H FDR method. \*\*\*p < 0.001. Pre, pre-DAA; Post, post-DAA; MHAI, modified hepatitis activity index; ALT, alanine transaminase; AST, aspartate aminotransferase; ALP, alkaline phosphatase; FFPE, formalin-fixed paraffin-embedded; PT, prothrombin time; INR, international normalized ratio.



nCounter analysis showed reduced antiviral and pro-inflammatory gene expression post-DAA therapy. (A) Cluster analysis of liver biopsy gene expression (controls (n = 9), pre-DAA (n = 17), and post-DAA (n = 14) patients). The heat map displays two primary clusters that predominantly represent pre-DAA samples and post-DAA/control samples. All clustering and label assignments were performed without reference to patient outcomes, ensuring that the definitions were unbiased and purely based on expression data. The dendrogram is presented as an exploratory tool to illustrate the structure of the data without overinterpreting the statistical robustness of each branch. (B) PCA of log2-transformed data confirmed this clustering. The colors represent the predefined experimental groups (ctrl, orange; pre-, light green; post-, brown), which were determined by study design and not based on post hoc unsupervised labels. (C) Volcano plots comparing pre-DAA vs. controls and pre- vs. post-DAA show antiviral/pro-inflammatory genes upregulated pre-DAA and returning to baseline post-treatment. (D) Differential gene expression obtained from comparing pre-DAA versus control groups was used to determine enriched pathways using DAVID software and the Reactome database. The y-axis represents the top enriched pathways; the dot color represents the log10 adjusted p-value, with yellow indicating higher significance (-log10 > 2 = ≤0.01). (E) Scatter plots show significant post-DAA downregulation of antiviral and type I IFN-induced genes, reaching control levels. Volcano plots show log2 fold change versus -log10 adjusted p-value (Benjamini-Yekutieli), with horizontal dashed lines indicating -log10 BY-adjusted p < 0.05 and vertical dashed lines representing  $\log 2$  fold change < -0.6 or > 0.6. Gene comparisons were analyzed using limma (R/Bioconductor), accounting for paired (pre/post) and unpaired samples with duplicateCorrelation function; linear models with empirical Bayes moderation were used, and p-values were adjusted by the B-H FDR method. \*p < 0.05; \*\*p < 0.01; \*\*\*p < 0.001; \*\*\*\*p < 0.0001. Ctrl, Controls; Pre, pre-DAA; Post, post-DAA; PCA, principal component analysis.

TABLE 1 Demographic and laboratory data for patients with HCV pre- and post-DAA treatment analyzed with nCounter and multiplexing imaging

Set #	Pt #	Pre/ Post	Age	Sex	F/P (m)	Dur. pre/ Post- Bx	Dur. SVR post-Bx	Ethnicity /Race	HCV Geno- type	HCV VL Log <sub>10</sub> IU/ mL	*** MHAI n/ 18	Fibrosis n/6	Fat (%)	*** ALT	*** AST	ALP	ALB	Tot BIL	PLT	PT	INR	Outcomes <sup>a</sup>	T cell panel	MAC panel	nCounter	DAA <sup>b</sup>
2/3	1	Pre	51- 60	М	68	54	14	NHW	1a	4.64	7	3	1	90	66	93	4.6	0.3	392	14.3	1.1	No Cirrhosis, No HCC	YES	YES	NA	Sofosbuvir/ simeprevir
1/ 2/3		Post	61- 70	-						SVR12	5	2-3	1	27	22	77	4	0.3	358	12.4	0.9		YES	YES	Post-cold	
2	2	Pre	41- 50	F	32	16	9	NHW	1a	5.39	9	2	40	352	361	140	4.1	0.8	157	13.4	1	No Cirrhosis, No HCC	NA	YES	NA	Sofosbuvir /ledipasvir
2		Post	41- 50							SVR12	4	2	20	22	16	136	4	0.5	223	12.6	0.9		NA	YES	NA	
2	3	Pre	41- 50	M	103	70	17	HW	1a	0.958	3	1	0	82	70	128	4.2	0.3	276	12.7	1	No Cirrhosis, No HCC	NA	YES	NA	Sofosbuvir/ simeprevir
2		Post	51- 60							SVR12	2	0-1	0	39	29	108	4.7	0.7	259	12.9	1		NA	YES	NA	
2	4	Pre	51- 60	F	142	85	28	NHW	2	0.664	8	6	5	239	168	94	4.3	1	101	15.4	1.2	HCC, Deceased	NA	YES	NA	Sofosbuvir/ ribavirin
2		Post	61- 70							SVR12	4	6	60	33	38	78	4	0.9	121	14.4	1.1		NA	YES	NA	
1/ 2/3	5	Pre	31- 40	М	111	20	19	NHAA	1a	2.61	4	1	0	40	29	108	4.4	0.5	322	12.7	0.9	No Cirrhosis, No HCC	YES	YES	Pre-cold	Sofosbuvir/ simeprevir
1/ 2/3		Post	31- 40							SVR12	1	1	0	25	25	114	4.9	0.1	344	12.7	1		YES	YES	Post-cold	
1/2	6	Pre	61- 70	М	105	15	6	HW	1a	3.08	2	1	0	28	30	123	4.1	0.7	197	13.3	1	No Cirrhosis, No HCC	NA	YES	Pre-cold	Sofosbuvir/ ledipasvir
1/2		Post	61- 70							SVR12	0	1	0	23	33	114	4.3	0.5	198	13.7	1.1		NA	YES	Post-hot	
1/2	7	Pre	51- 60	F	113	26	24	NHW	1b	3.32	5	3	10	48	53	138	4.4	0.8	194	12.2	0.9	No Cirrhosis, No HCC	NA	YES	Pre-cold	Sofosbuvir/ simeprevir
1/2		Post	51- 60							SVR12	2	1	10	30	25	120	4	0.3	210	13.8	1.1		NA	YES	Post-cold	
1/2/3	8	Pre	51- 60	М	128	24	20	NHW	2b	17.2	3	2	15	15	23	99	4	0.5	159	12.6	0.9	No Cirrhosis, No HCC	YES	YES	Pre-cold	Sofosbuvir/ ribavirin
1/2/3		Post	51- 60							SVR12	2	1	5	33	24	105	4.5	0.6	200	12.3	0.9		YES	YES	Post-cold	
	9	Pre	51- 60	М	84	NA	26	NHW	2b	3.96	NA	NA	NA	35	32	63	4.4	0.6	145	13	1	No Cirrhosis, No HCC	NA	NA	NA	Sofosbuvir/ simeprevir
1		Post	51- 60							SVR12	1	1-2	10	48	38	55	4.3	0.9	240	12.7	1		NA	NA	Post-cold	

(Continued)

frontiersin.org

Millian et al.

TABLE 1 Continued

Set #	Pt #	Pre/ Post	Age	Sex	F/P (m)	Dur. pre/ Post- Bx	Dur. SVR post-Bx	Ethnicity /Race	HCV Geno- type	HCV VL Log <sub>10</sub> IU/ mL	*** MHAI n/ 18	Fibrosis n/6	Fat (%)	*** ALT	AST	ALP	ALB	Tot BIL	PLT	PT	INR	Outcomes <sup>a</sup>	T cell panel	MAC panel	nCounter	DAA <sup>b</sup>
1	10	Pre Post	41- 50	F	45	21	15	NHAA	1b	2.94	8	4-5	5	122	133	187	4.3	0.8	179	13.2	1	ChCA, Deceased	NA	NA	Pre-hot	Viekira Pak
1			41- 50							SVR12	3	4	2	10	20	135	4	0.5	247	13.8	1.1		NA	NA	Post-cold	
1	11	Pre Post	51- 60	F	56	24	86	Н	1a	0.011	4	3	10	27	23	102	2.3	0.3	298	13.9	1.1	No Cirrhosis, No HCC	NA	NA	Pre-hot	Elbasvir/ grazoprevir
1			51- 60							SVR12	2	3	5	18	13	104	4.1	0.7	261	13.9	1.1		NA	NA	Post-cold	
1/3	12	Pre	51- 60	М	100	34	26	W	1a	0.22	3	2-3	5-10	35	21	69	4.2	0.3	289	12.2	0.9	No Cirrhosis, No HCC	YES	NA	Pre-hot	Sofosbuvir/ ledipasvir
1/3		Post	51- 60							SVR12	2	2-3	5-10	25	16	121	4.7	0.5	328	9.1	0.8		YES	NA	Post-hot	
1/3	13	Pre	41- 60	М	103	45	31	HW	1a	0.053	5	5	5	51	46	120	4.7	0.7	198	14.6	1.1	Cirrhosis	YES	NA	Pre-hot	Viekira Pak
1/3		Post	51- 60							SVR12	2	4-5	0	20	19	141	4.3	0.3	195	10.4	1		YES	NA	Post-cold	+ribavirin
1	14	Pre	61- 70	М	54	NA	NA	AA	1a	4.94	7	3	0	21	20	67	3.8	0.4	185	12.1	0.9	Deceased	NA	NA	Pre-hot	No Tx <sup>c</sup>
1	15	Pre	51- 60	М	96	NA	NA	AA	1a	2.49	2	1	0	27	44	121	4.1	3.9	257	12.4	0.9	No Cirrhosis, No HCC	NA	NA	Pre-cold	Sofosbuvir/ velpatasvir
1	16	Pre	51- 60	F	94	NA	NA	W	1b	0.20	4	2	15	58	70	192	4.3	0.7	274	12.4	0.9	No Cirrhosis, No HCC	NA	NA	Pre-cold	Sofosbuvir/ ledipasvir
1	17	Pre	51- 60	М	131	NA	NA	W	2b	2.33	4	2-3	0	44	44	88	4.7	1.2	196	22	1.9	Cirrhosis, Deceased	NA	NA	Pre-cold	Sofosbuvir/ velpatasvir
1	18	Pre	51- 60	F	39	NA	NA	W	2b	0.034	3	1-2	0	45	32	78	4.6	0.5	482	12.7	1	No Cirrhosis, No HCC	NA	NA	Pre-cold	Sofosbuvir/ velpatasvir
1	19	Pre	61- 70	М	79	68	62	W	3a	ND	7	4-5	0	47	37	74	4.4	0.9	193	12.7	0.9	Cirrhosis, HCC, Deceased	NA	NA	Pre-hot	Sofosbuvir/ daclatasvir
1		Post	61- 70							SVR12	3	4-5	0	19	36	61	4.1	0.7	148	12.1	1.1		NA	NA	Post-cold	/ribavirin
1	20	Pre	51- 60	F	161	125	17	AA	1a	0.20	4	1	5	95	80	86	3.2	0.3	179	13.3	1	Cirrhosis	NA	NA	Pre-hot	Sofosbuvir/
1		Post	61- 70							SVR12	4	5	15	28	38	180	4.2	0.4	223	11.9	1		NA	NA	Post-cold	velpatasvir
1	21	Pre	51- 60	М	77	57	9	AA	1a	0.73	7	3	0	107	85	160	4.4	0.9	189	13	1	No Cirrhosis, No HCC	NA	NA	Pre-hot	Glecaprevir/ pibrentasvir
1		Post	51- 60							SVR12	2	2-3	1	31	62	97	4.4	1	157	11	1		NA	NA	Post-cold	

FABLE 1 Continued

DAAb	Peg- Ribavirin <sup>d</sup>	
nCounter	Pre-hot	Post-hot
MAC	NA	NA
T cell panel	NA	NA
PLT PT INR Outcomes <sup>a</sup>	Cirrhosis	
N R	1.3	1.1
F	16.5 1.3	152 14.4 1.1
PLT	193	152
ALB Tot BIL	0.8	0.5
ALB	2.7	3.3
ALP	92	186
AST	14 15	28
ALT	14	40
Fat	0	0
Fibrosis n/6	3-4	5-6
*** MHAI n/ 18	r	4
HCV VL Log <sub>10</sub> IU/ mL	ND	SVR12
HCV Geno-type	1b	
Ethnicity /Race	HW	
Dur. SVR post-Bx	S	
Dur. pre/ Post- Bx	7	
F/P (m)	21	
Sex	M	
Age	41-	41-
Pre/ Post	Pre	Post
<b>۲</b> #	22	

Set 1: Patients included in the gene expression analysis (nCounter). Set 2: Patients analyzed using multispectral imaging microscopy with the T cell panel. Normal range: ALT, 9-51 U/L; AST, 13-40 U/L; ALP, 34-122 U/L; ALB, 3.5-5 g/dL; Tot BIL, 0.1-1.1 mg/dL; PLT,166-358 x1000/µL; PT, 11-13.5 sec; INR, 0.8-1.2

Abbreviations: Pt #, patient number; Pres. pre-treatment; Post-vestment; Post-\*\*, patients with persistent inflammation post-DAA by histopathology (MHAI>2); M, male; F, female; F/P, Follow-up (months); Dur. (Pre/Post Bx), Duration SVR Post-therapy biopsy virus; VL, viral load; Tot BIL, total bilirubin; PLT parameters were analyzed with limma (R/Bioconductor), accounting for paired and unpaired samples with within-patient correlations. Moderated t-statistics were computed, and p-values were adjusted for multiple testing using the Benjamini-Hochberg method ND, not detected. white; NHAA, Non-Hispanic African macrophage; DAA, Direct-acting antivirals; NA, not available; months); Dur. SVR Post-Bx, Duration SVR12, undetectable HCV RNA in

Asterisk on top of MHAI, ALT, and AST represent significant statistical differences between the groups (\*\*\*p < 0.001). Superscript a. Patient 4 and 10 succumbed to HCC and ChCA, respectively, while patients 14 and 19 died of cirrhosis-related complications. Patient 13

lied of cardiogenic shock. b: All patients completed the duration of the treatment according to the

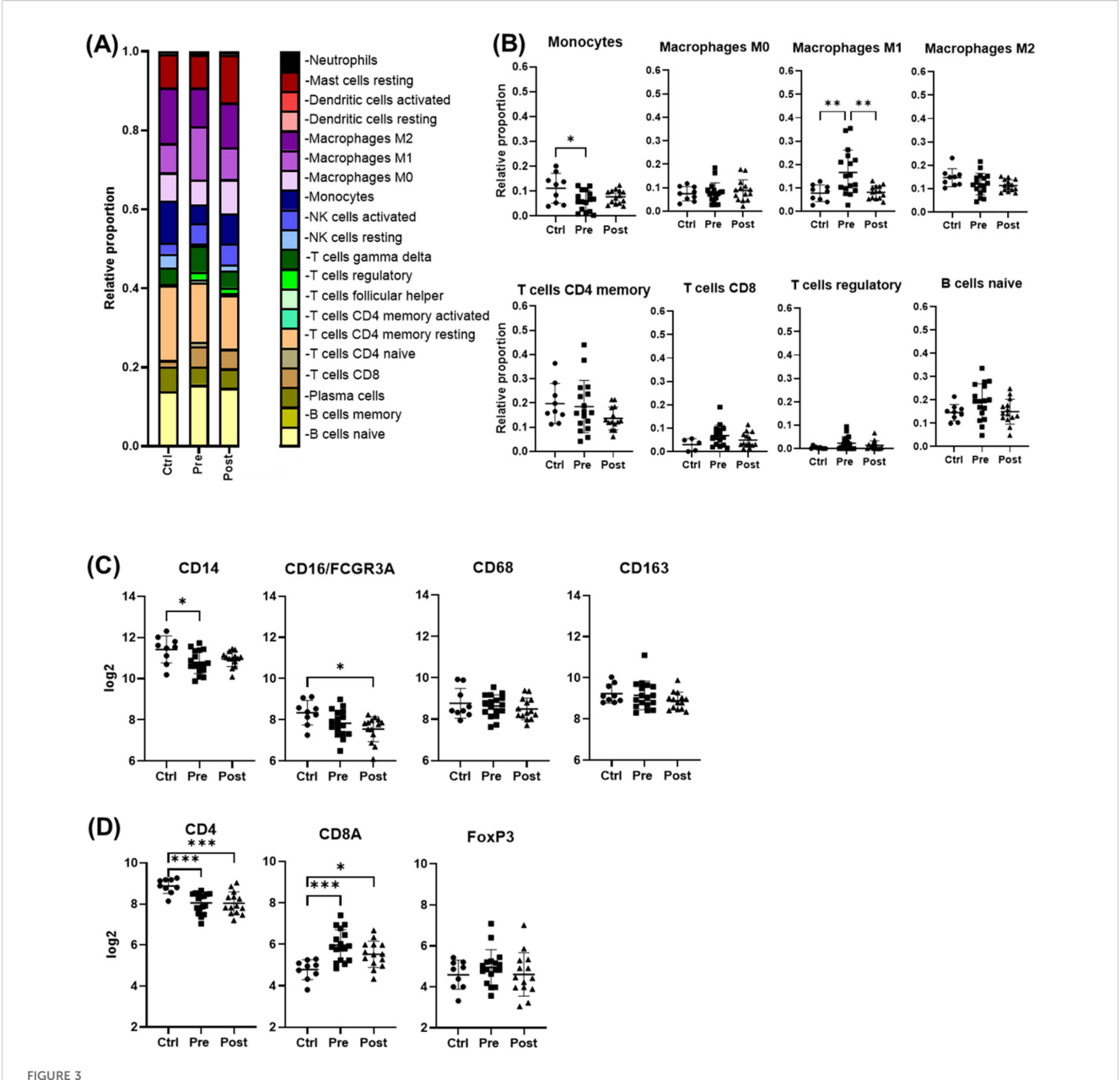
guidelines at the time of treatment except patients 22 and 14. c. Patient did not receive any treatment, d: Treatment was discontinued after 5 weeks due to renal

Huang et al., 2022) (Figures 4A, C-E; Supplementary Figures S2, S3A-F, S4A-D; Supplementary Tables S7-S9). In contrast, pre-cold patients retained antiviral and innate immune responses without marked inflammation, representing a distinct immunological profile (Figures 4A, C-E; Supplementary Figures S2-4, Supplementary Table S10). No statistically significant differences were observed in histopathological features (MHAI and fibrosis) or laboratory values when compared Pre-hot with the pre-cold group (Supplementary Figure S2). Similarly, a post-DAA group formed two subclusters: post-hot (n = 3) clustering along with the pre-hot subcluster, and post-cold (n = 11) near the control group (Figure 2B; Supplementary Figures S3B, D). Post-hot patients exhibited persistent immune regulation and activation of oncogenic pathways (TGFβ1 and CD24) with downregulation of complement (C8B, CFB, C1S, SERPING1, C3, CD46, CD81, CD40) and fibroblast proliferation genes (PDGFC, BMI1, FN1, SMAD2), implying potential ongoing tissue remodeling (Figures 4B-E; Supplementary Figure S3; Supplementary Tables S11, S12). Cell deconvolution analysis further showed that M1 macrophages were significantly elevated in the pre-hot group compared to the pre-cold group (p < 0.01) and decreased following treatment (Figure 4B). Additionally, activated NK cell and naive B cell proportions were significantly increased pre-DAA (p < 0.01) compared to controls, suggesting continued immune engagement. Post-cold patients, in contrast, closely resembled controls, indicating immune normalization (Figures 4F, G; Supplementary Figures S1B, S2, S3; Supplementary Table S13).

The heatmap in Figure 5 summarizes activated relevant pathways in each subcluster. The pre-hot group showed stronger gene upregulation than the pre-cold group, enriched in type I/III interferon and antiviral response pathways. After achieving SVR, post-DAA patients showed reduced innate immune and antiviral gene expression. Still, post-hot patients retained mixed activation of inflammatory (TNF, TLRs,  $NF\kappa B$ ) and anti-inflammatory/profibrotic ( $TGF\beta$ , IL-4, IL-13, STAT6) pathways.

# Anti-inflammatory macrophages are the predominant phenotype in the hepatic microenvironment after DAA therapy

Multiplex imaging provided insight into hepatic macrophage population shifts. CD14+ macrophages, the predominant subtype in controls, along with their subpopulations (e.g., CD14+/CD16+, CD14+/CD163+, CD14+/Mac387+) were significantly decreased during chronic infection (pre-DAA) and declined further following DAA treatment (p < 0.05) (Figures 6A-C) (Saldarriaga et al., 2020; Saldarriaga et al., 2024). Resident (CD68+ and CD68 +/CD163+) increased pre-DAA (p < 0.05), and decreasing considerably post-DAA, suggesting a resolution of inflammation following viral clearance. Anti-inflammatory macrophages CD16+ and their subpopulations (e.g., CD16+/CD163+, CD16+/CD68+) significantly increased post-treatment (p < 0.05), indicating a shift toward immune resolution and tissue remodeling (Figures 6A-C). These results are consistent with the gene expression analysis, which indicated a significant reduction in inflammatory macrophages (M1) following treatment (Figures 3B).



Cell deconvolution analysis reveals distinct immune cell dynamics post-DAA therapy. Gene expression was analyzed using CIBERSORT (Chen et al., 2018). We applied this tool, which uses a reference dataset of gene expression signatures from known cell types, to estimate the relative proportions of different immune cell types in liver biopsies from controls (n = 9) compared with those from patients pre- (n = 17) and post-DAA treatment (n = 14).

(A, B) CIBERSORT showed individual variation in macrophage and T cell populations. M1 macrophages significantly decreased post-DAA, resembling controls. Pre-DAA enriched M1 and T cell genes are shown in Supplementary Figure S1A. (C, D) Box plots compare log2 gene expression of resident, pro-inflammatory, and anti-inflammatory macrophages, and T cell markers among the groups. Gene expression was analyzed using limma (R/ Bioconductor), accounting for paired (pre/post) and unpaired samples with duplicateCorrelation function; linear models with empirical Bayes moderation were used, and p-values were adjusted by the B-H FDR method. \*p < 0.05; \*\*p < 0.01. Ctrl, Controls; Pre, pre-DAA; Post, post-DAA.

# Spectral imaging revealed significant heterogeneity and diverse hepatic T cell populations in both pre- and post-DAA groups

Before treatment, biopsies revealed largely heterogeneous distributions of analyzed T cell populations and their subpopulations across pre- and post-treatment groups. Several

populations and subsets, including CD3+, FoxP3+, CD4+/CD45R0+ were modestly elevated in the pre-treatment group, but these trends were not statistically significant and were not different post-treatment (Figures 7A–C). Importantly, four out of five patients analyzed by spectral imaging (Table 1, subset 3) had persistent hepatic inflammation by histology, consistent with the lack of measurable recovery of T cell subsets. Inter-individual variability and the small sample size likely limited detection, and

multiple testing adjustments across T cell phenotypes yielded no significant differences. Persistent portal inflammation (MHAI > 2) was observed in 14 of 17 patients (82.3%, 95% CI: 64.2–100%) post-DAA, indicating residual or ongoing lymphocytic infiltration (Table 1). Patient 1, for instance, displayed post-treatment

inflammation (MHAI > 2), with increased proportions of single-positive CD3+ and CD45RO+ cells, as well as double-positive CD3+/CD45RO+ memory T cells within the liver (Figure 7A). Controls (n = 2) were shown for descriptive purposes only and not included in statistical analysis. These findings highlight the persistence of

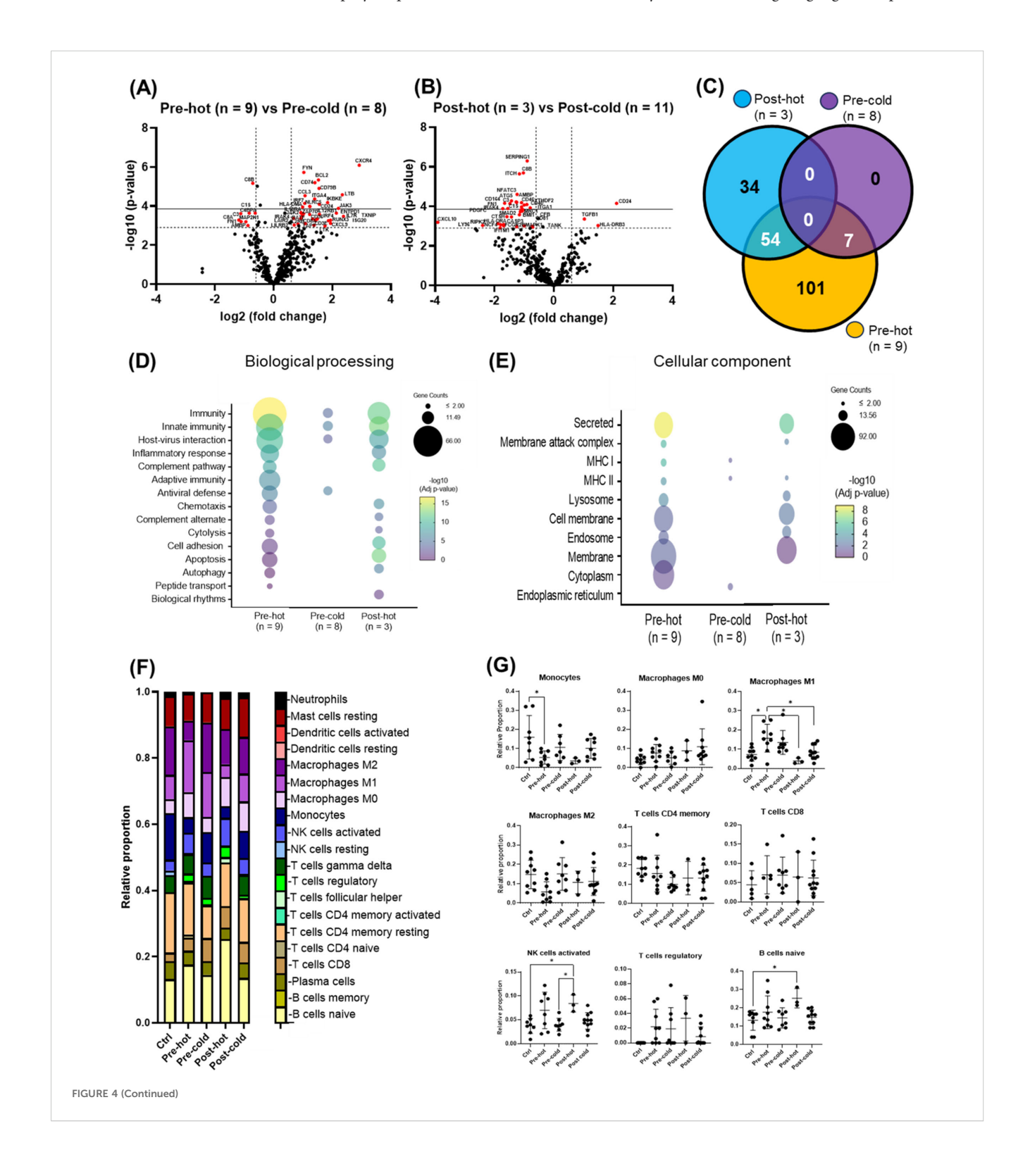


#### FIGURE 4 (Continued)

Gene expression patterns within the pre- and post-DAA groups revealed distinct individual responses to HCV infection and DAA therapy. In patients infected with HCV and then treated with DAA (see Figure 2A), we identified different subclusters in the heat map: pre-hot (high expression pre-DAA vs. controls), pre-cold (low expression pre-DAA vs. controls), post-hot (high expression post-DAA, like pre-hot), and post-cold (low expression post-DAA, like controls). (A. B) Volcano plots compare gene expression in pre-hot vs. pre-cold and post-hot vs. post-cold groups. (C) The Venn diagram illustrates significantly expressed genes across pre-cold, pre-hot, and post-hot patients and their overlap. Of the 197 differentially expressed genes (the pre-hot expressing 162 genes), 54 genes overlap between the post-hot and pre-hot groups, while seven genes overlap between the pre-cold and pre-hot groups. In addition, the pre-cold showed a gene expression pattern like the controls, as it had the fewest significant genes (7 genes) compared to the other groups. (D, E) Differential gene expression obtained from comparing pre-hot, pre-cold, and posthot groups versus liver controls (see Supplementary Figures S3, S4; Supplementary Table S8, S10, S12) was used to determine enriched pathways using DAVID software and the Reactome database. The y-axis represents the top enriched pathways. The color of the dots represents the -Log10 of the adjusted p-value obtained from the enrichment analysis. -Log10 > 2 (adjusted p-value = <0.01) indicates significant enrichment (yellow dots represent higher significance). Compared to the pre-hot group, the post-hot group was characterized by activating persistent immune and inflammatory response pathways without activating antiviral genes and MHC I pathways. (F, G) Gene expression was analyzed using CIBERSORT to estimate the relative proportions of different immune cell types in controls and pre- and post-DAA treatment groups (pre-hot, pre-cold, post-hot, and post-cold). Pre-hot patients showed increased proportions of M1 macrophages, activated NK cells, and naïve B cells. Specific macrophage (M1 and M2), T and B cells, and NK cells genes enriched in each group are shown in Supplementary Figures S1A, B, with corresponding laboratory values in Supplementary Figure S2. Additional volcano plots and contributing genes are in Supplementary Figure S3 and Supplementary Tables S7-S13. Volcano plots show log2 fold change versus -log10 adjusted p-value (Benjamini-Yekutieli), with horizontal dashed lines indicating -log10 BYadjusted p < 0.05 and vertical dashed lines representing log2 fold change < -0.6 or > 0.6. Gene expression was analyzed using limma (R/ Bioconductor), accounting for paired (pre/post) and unpaired samples with duplicateCorrelation function; linear models with empirical Bayes moderation were used, and p-values were adjusted by the B-H FDR method. \*p < 0.05; \*\*p < 0.01; \*\*\*p < 0.001; \*\*\*\*p < 0.001; \*\*\*\*p < 0.001.

hepatic inflammation in treated HCV patients, underscoring that the immune microenvironment remains variably activated across individuals despite viral clearance. Consistent with our spectral imaging results, T cell populations (CD8+) and specific genes (*CD8A*) remain elevated post-treatment (Figures 3A–C). In agreement with previous reports of persistent

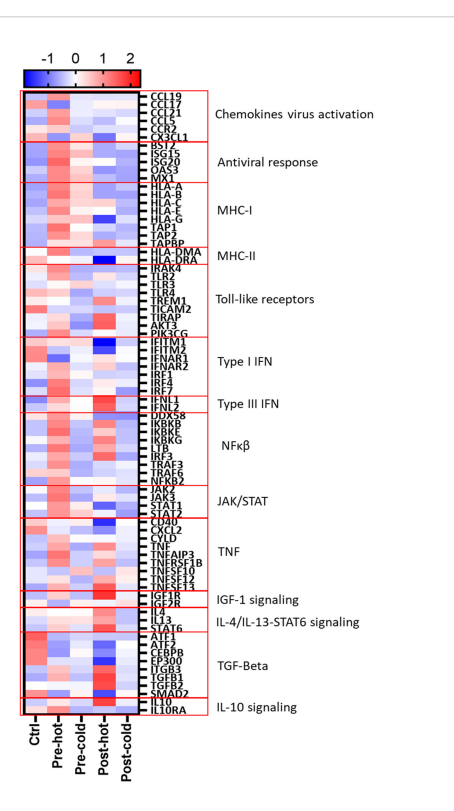


#### FIGURE 5

Gene expression patterns reveal distinct inflammatory and fibrogenic pathways despite DAA therapy. Differentially expressed genes (Supplementary Tables S8–S13; pre-hot, pre-cold, post-hot, and post-cold groups compared to controls) were analyzed using STRING network clustering (MCL inflation = 5) and visualized in a heatmap using the average Z-score value (intensity range:  $\pm$  2) for each group. Red boxes highlight key pathway clusters. Antiviral response and MHC-I markers were only upregulated in pre-DAA groups (pre-hot and pre-cold). Inflammation in both pre-DAA groups was linked to type I interferon and TNF/NF $\kappa$ B signaling, with lower expression in the pre-cold group. The post-hot group showed upregulation of inflammatory pathways, including TNF/NF $\kappa$ B, and anti-inflammatory and profibrotic pathways, such as TGF- $\beta$ 1/2 and IL-4/IL-13/STAT6. pre-hot, high gene expression pre-DAA; pre-cold, low gene expression post-DAA; Ctrl, controls.

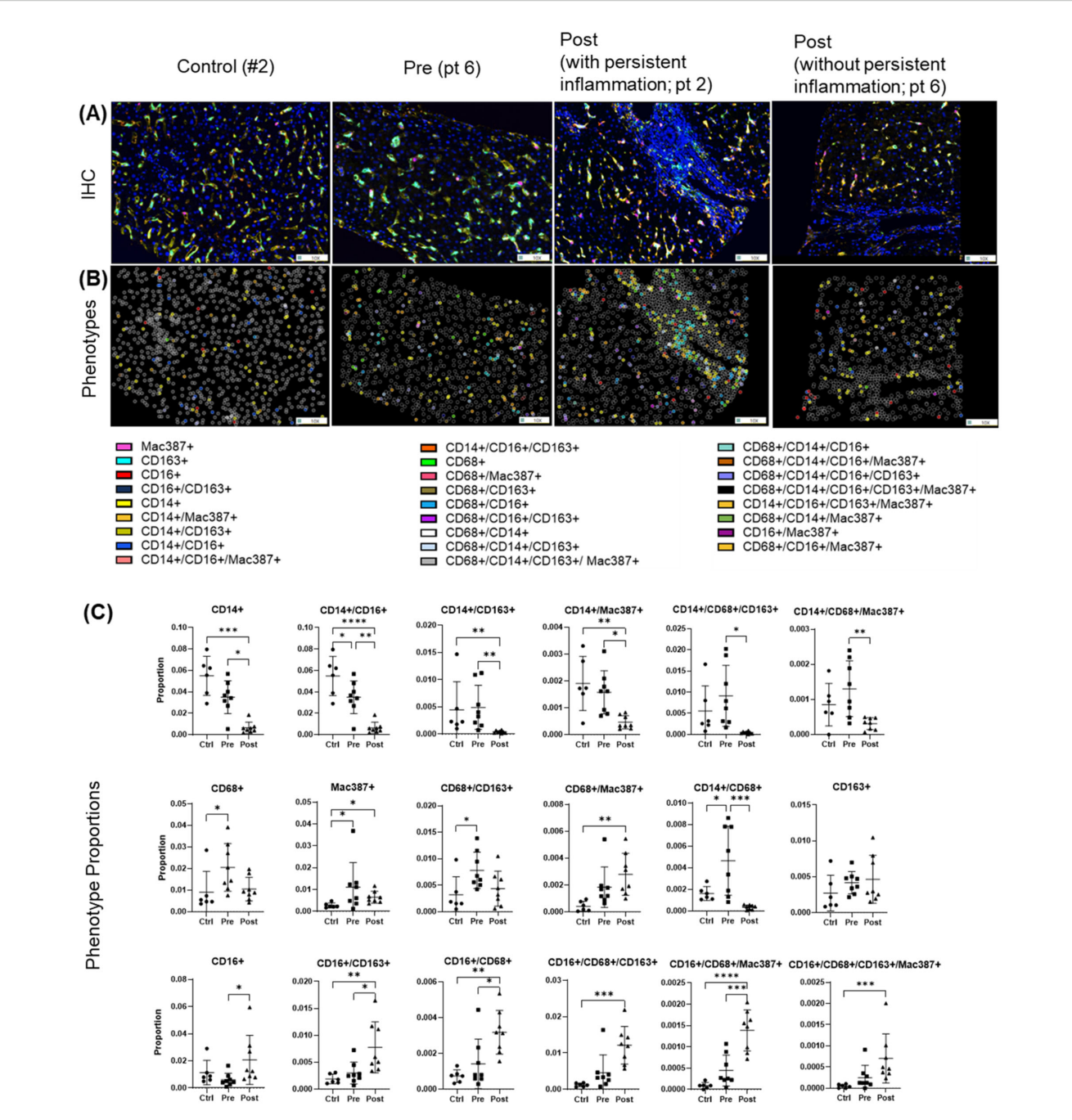


FIGURE 6

Macrophage phenotypes in liver biopsies pre- and post-DAA therapy reveal a dominant anti-inflammatory response post-treatment. Biopsies were stained with the macrophage multiplex panel (CD68, CD14, CD16, CD163, Mac387, and DAPI), and images from the stained slides were acquired using the Vectra 3 automated quantitative pathology imaging system. Multicomponent TIFF images were analyzed with Visiopharm using optimized custom AI applications to determine the type and number of macrophage phenotypes in the hepatic microenvironment (controls, n=6; patients with HCV pre-DAA, n=8; and post-DAA, n=8). (A) Representative multiplex images and (B) phenotypes from controls, a pre-DAA patient, and two post-DAA patients (with: MHAI > 2 and without: MHAI < 1, persistent inflammation). Each colored dot represents a unique cellular phenotype, and gray dots represent negative cells for all the markers evaluated. (C) Scatter plots were used to compare the proportions of specific cell populations across control, pre-DAA, and post-DAA groups. Control patients exhibited a higher abundance of CD14+ cells, which decreased with HCV infection. Pre-DAA patients showed an increase in inflammatory macrophages (CD68+, CD14+, Mac387+, CD68+/CD14+) compared to controls, which generally diminished after DAA treatment, except in one patient (pt 2), who exhibited persistent inflammation. In contrast, post-treatment samples showed increased anti-inflammatory macrophages (CD16+ and CD16+/CD163+) populations. Images were acquired at 20X. Statistical comparisons were performed using paired or unpaired t-tests, with p-values adjusted for multiple comparisons by the Bonferroni method. \*p < 0.05; \*\*p < 0.01; \*\*\*p < 0.001, \*\*\*\*p < 0.001.

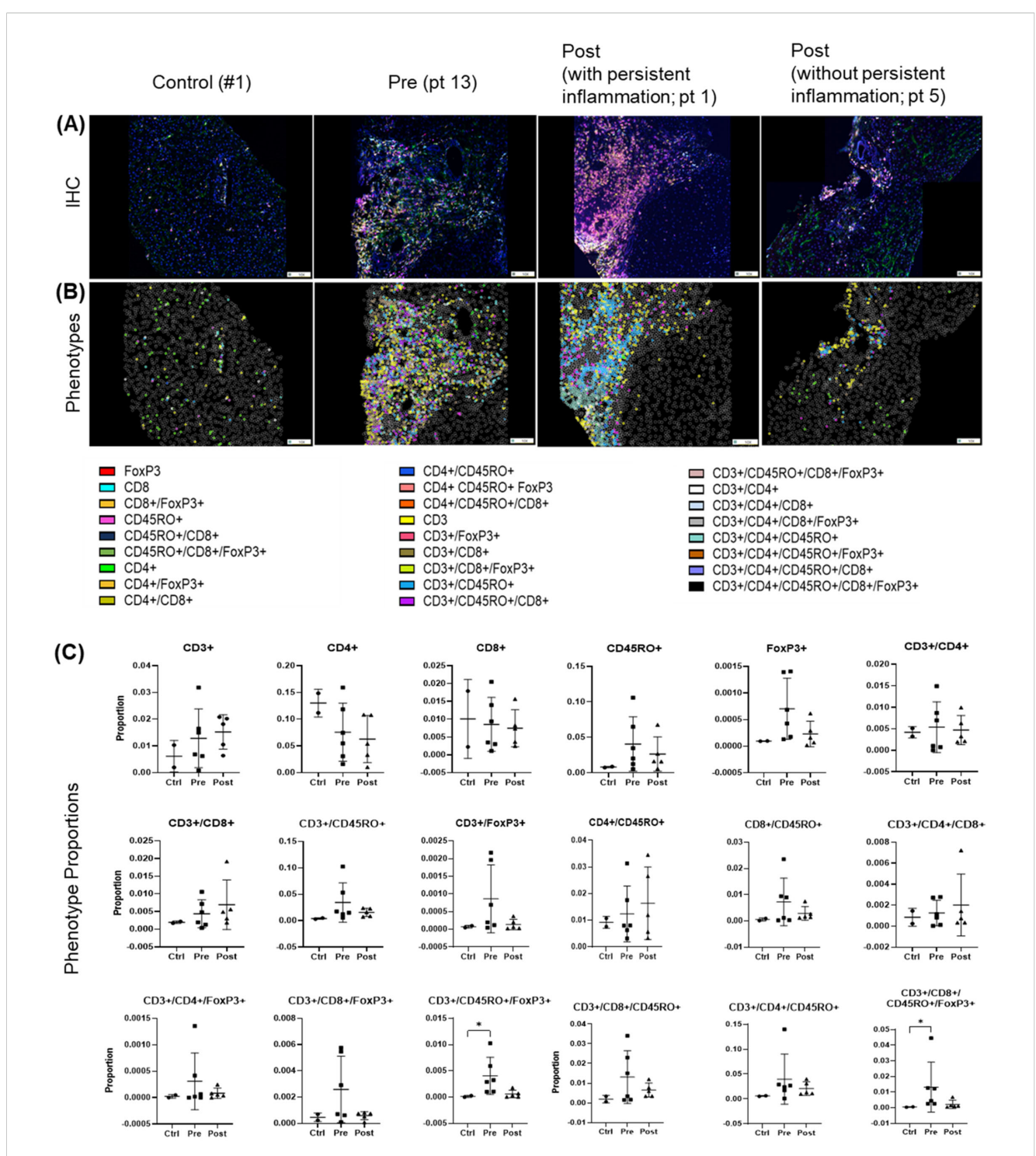


FIGURE 7

T cell phenotypes in liver biopsies pre- and post-DAA therapy show individual heterogeneity. Biopsies were stained with a multiplex T cell panel (CD3+, CD4+, CD8+, CD45RO+, FoxP3+, and DAPI), and images from the stained slides were acquired using the Vectra 3 automated quantitative pathology imaging system. Multicomponent TIFF images were analyzed with Visiopharm using optimized custom AI applications to determine the type and number of T cell phenotypes in the hepatic microenvironment (controls, n = 2; patients with HCV pre-DAA, n = 5; and post-DAA, n = 5).

(A, B) Representative multiplex images from controls, a pre-DAA patient, and two post-DAA patients (with: MHAI > 2 and without: MHAI < 1, persistent inflammation). Each colored dot represents a unique cellular phenotype, and gray dots represent negative cells for all the markers evaluated. (C) Scatter plots were used to compare the proportions of specific T cell populations across pre-DAA and post-DAA groups. Individual heterogeneity was evident in the pre- and post-DAA groups, with a predominant mixed lymphocytic infiltrate (helper/CD4+, cytotoxic/CD8+, and memory/CD45RO+) before treatment and a mixed memory phenotype (CD3+, CD45RO+, CD3+/CD45RO+, CD4+/CD45RO+, CD3+/CD4

+/CD45RO+) post-treatment in patients with persistent inflammation. MHAI, modified hepatitis activity index; AI, artificial intelligence. Statistical comparisons were performed using paired t-tests, with p-values adjusted for multiple comparisons by the Bonferroni method. Controls (n = 2, shown for descriptive purposes only; not included in statistical analysis).

portal tract inflammation (Welsch et al., 2017; Putra et al., 2018; Hsieh et al., 2021; Saldarriaga et al., 2021) our analysis of T cell-related gene and marker expression before and after treatment indicates that lymphocytic persistence within the liver can occur despite successful viral clearance. Similarly, *CD4* gene expression was reduced pre-DAA, likely reflecting clonal exhaustion and deletion of HCV-specific CD4 T cells, and did not significantly recover post-SVR (Figure 3D). Although HIV coinfection in some patients may potentially influence *CD4* expression (Gazzola et al., 2009; Corbeau and Reynes, 2011; Young et al., 2012), no significant differences were observed between patients with (pt 2-3, 5-13, 15) and without (pt 1, 4, 14, 16-22) HIV coinfection (Supplementary Figure S5A).

# Gene expression and histopathology before DAA treatment and their associations with clinical outcomes

Two pre-DAA subclusters based on gene expression were identified as mentioned above: the pre-hot subcluster (nine out of 17, 52.9%) with enriched gene expression and the pre-cold subcluster (eight out of 17, 47.1%) with low gene expression (Figures 2, 4; Supplementary Tables S7–S10). Although the pre-hot subcluster exhibited a trend toward higher MHAI scores, fibrosis stage, and ALT and AST levels, no statistically significant differences were observed between the pre-hot and pre-cold subclusters in these or other clinical parameters (Supplementary Figure S2; Table 1).

Using Fisher's exact test, we observed a significant positive association between the pre-hot gene expression profile and adverse outcomes (OR = 14.0, 95% CI: 1.31-178.5; p=0.049) that included cirrhosis, HCC, or liver failure-related death. After adjustment for baseline fibrosis stage, MHAI, and HIV infection status, the pre-hot group remained associated with higher odds of poor outcomes (adjusted OR = 8.04, 95% CI: 0.18-2123.07), although this association was no longer statistically significant (p=0.328) (Figure 8A). Among pre-hot patients, 44.4% (four out of nine) developed cirrhosis, and 33.3% (three out of nine) died from decompensated cirrhosis, compared to only one adverse outcome, 12.5% (one out of eight) in the pre-cold group (Table 1).

Among the 16 patients with paired liver biopsies, the fibrosis stage either worsened or remained similar in the pre-hot subcluster. At the same time, fibrosis consistently decreased or remained low in the pre-cold group after DAA treatment (Figure 8B). Patients with adverse outcomes had significantly higher MHAI scores (p < 0.05) and fibrosis stages (p < 0.01) pre- treatment than those with favorable outcomes, although ALT levels and viral load did not differ significantly (Figure 8C, Table 1). To further explore predictive value, we assessed whether MHAI scores and fibrosis stages at baseline could predict outcomes. Each unit increase in MHAI score was associated with nearly double the odds of poor outcomes (OR = 1.90, 95% CI: 0.72-6.34), although this did not reach statistical significance (p = 0.215). Similarly, higher fibrosis stages showed a trend toward poor outcomes (OR = 1.65, 95% CI:

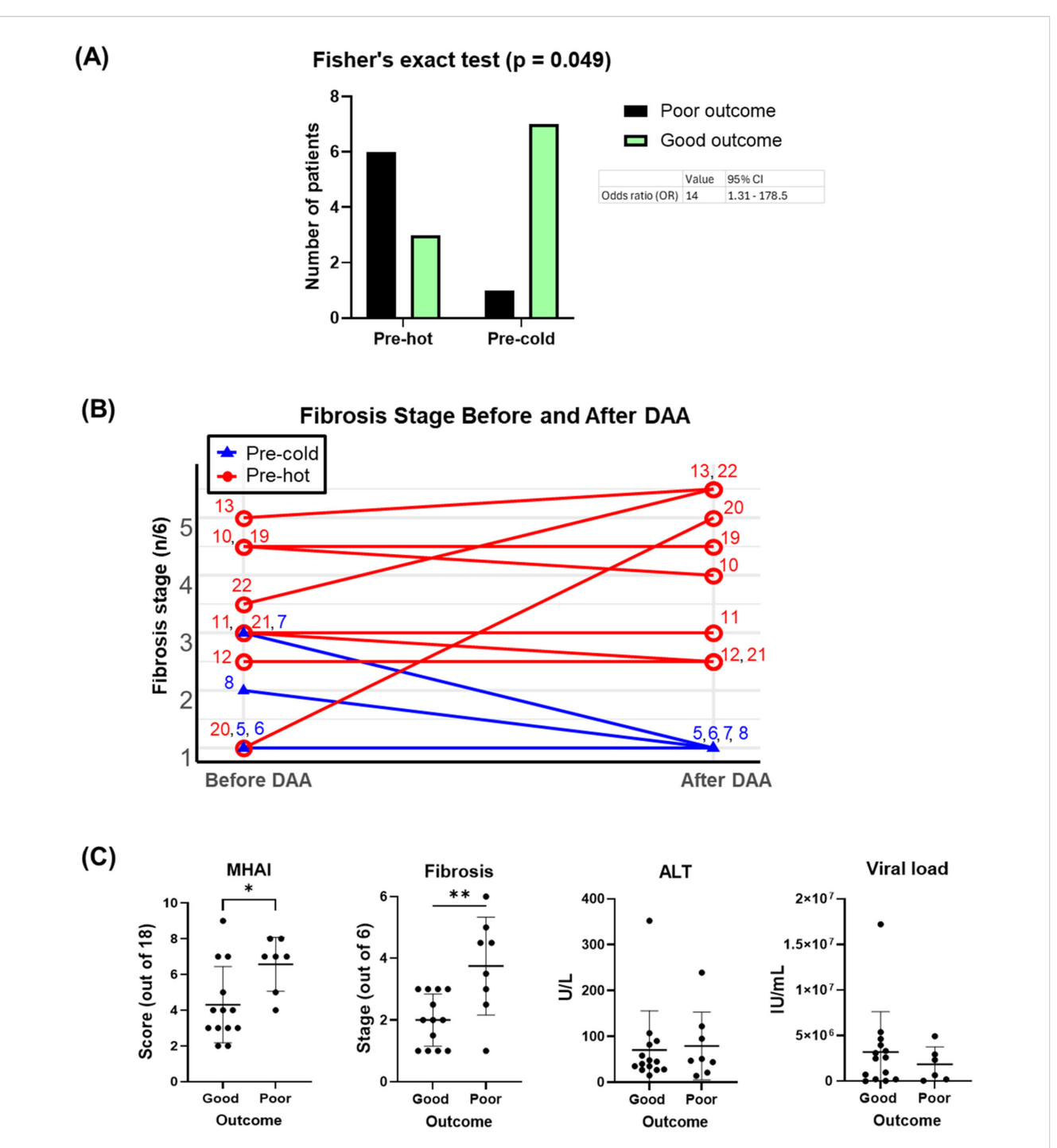
0.44-9.97) but were not statistically significant predictors (p = 0.488), likely reflecting the limited sample size and wide variability.

### Discussion

While HCV is now curable in most individuals (Oru et al., 2021), the risk of liver-related complications remains, particularly in patients with advanced fibrosis or cirrhosis (Saldarriaga et al., 2021). Persistent lymphocytic portal tract inflammation posttreatment has been noted by us and others (Putra et al., 2018; Hsieh et al., 2021; Saldarriaga et al., 2021), raising questions about its clinical implications. Macrophages and T cells play a crucial role in the immune response to HCV, but chronic infection impairs macrophage activation and leads to T cell dysfunction (Tu et al., 2010; Ahmed et al., 2019; Vranjkovic et al., 2019; Zhao et al., 2022). While fibrosis progression is more strongly associated with host factors such as sex, age, and alcohol consumption than with inflammatory activity or viral load (Poynard et al., 1997; Fattovich et al., 2004), the role of immune cell dynamics, particularly post-treatment, remains poorly understood. To address this, we analyzed liver biopsies taken before and after DAA therapy, compared them to those of uninfected controls, and correlated the findings with clinical outcomes.

All patients achieved SVR, with normalized transaminases and reduced inflammation per MHAI scoring. However, unlike other studies, we did not observe a significant reduction in fibrosis after viral clearance (Figure 1; Table 1) (D'Ambrosio et al., 2012; Bility et al., 2016). HCV infection triggered a potent interferon (IFN)-mediated immune response, which declined following DAA treatment in most patients, reaching levels comparable to those of uninfected controls (Figure 2E; Supplementary Figure S3D). DAAs are known to suppress ISGs and antiviral pathways in hepatic immune cells (Boldanova et al., 2017; Holmes et al., 2019; Burchill et al., 2021; Listopad et al., 2022; Cui et al., 2024), whether this immunologic shift affects long-term liver health remains uncertain. Unlike IFN-based therapies, DAAs achieve better normalization of these immune responses (Hou et al., 2014).

We observed a significant decrease in inflammatory macrophages (M1-like) following treatment (Figures 3, 6). HCV drove the upregulation of M1-associated markers (e.g., CD80, CCL5, CXCL9), which declined after treatment (Figure 3B; Supplementary Figure S1A). HCV infection elicits dynamic changes in hepatic myeloid cell subsets, particularly CD14+ and CD16+ macrophages, contributing to the entire pool of ISG and MHC-II genes expressed during infection (Cui et al., 2024). Protein analysis in the imaging subset supported a shift from proinflammatory to anti-inflammatory macrophage phenotypes, as CD14+ cells declined while CD16+ cells predominated post-SVR (Figure 6C). The persistence of CD16-expressing subsets, often at higher levels than in uninfected controls, aligns with reports of an expanding CD16 population after DAAs (Cui et al., 2024). Spectral imaging revealed a significant decrease in CD14+/CD163+ macrophages following DAA and an increase in CD16+/CD163+



Associations of pre-DAA gene expression profile (Pre-hot and Pre-cold) and baseline histopathology (MHAI, Fibrosis) with clinical outcomes. (A) Adverse outcomes occurred more frequently in the pre-hot (seven out of nine, 77.7%) compared to the pre-cold group (one out of eight, 12.5%). Pre-hot gene expression was associated with higher odds (OR: 8) of adverse outcomes although this association was not significant after adjustment for baseline factors such as MHAI and fibrosis. (B) Twelve patients with paired liver biopsy samples (pre- and post-treatment) and gene expression profiling (pre-hot and pre-cold) were analyzed. Increased gene expression (pre-hot; pt 10-13, 19-22) before treatment did not improve their fibrosis post-DAA, while it consistently remained low in the pre-cold group (pt 5-8). (C) Patients with adverse (poor) clinical outcomes had significantly higher MHAI scores and fibrosis stages at baseline compared to patients with favorable (good) outcomes, but neither variable was a statistically significant predictor of outcomes in regression analyses. Abbreviations: MHAI, modified hepatitis activity index. The Fisher exact test assessed gene expression-outcome association (OR >1 = positive association) To assess potential confounding variables affecting outcomes (poor vs. good), we performed multivariable logistic regression in R, adjusting for baseline fibrosis stage, MHAI scores, and HIV status. Group differences were analyzed using unpaired t-test or the Mann-Whitney test. \*p < 0.05; \*\*p < 0.01; \*\*\*p < 0.001.

subsets (Figure 6C), highlighting the advantages of assessing tissue protein expression.

Two distinct pre-treatment inflammatory profiles were identified by gene expression analysis: a "pre-hot" subcluster with high expression of pro-inflammatory (NLRP3, TLR2-4, NFKB, Jak2-3/STAT1-2, TNF) and antiviral (ISG15/20, MX1, OAS3) genes, as well as type I/III IFNs (IFITM1-2, IFNAR1-2, IRF1,4, IFNL1-2) and antigen presentation markers (HLA-C, TAP1-2, HLA-DMA, HLA-DRA); and a "pre-cold" subcluster with lower-level expression (Figures 2, 4; Supplementary Tables S7–S10). While host IFN-λ3/ 4 gene variants influence ISG expression, HCV pathogenesis, and response to treatment (Terczyńska-Dyla et al., 2014; Salum et al., 2020), we did not assess genetic variations in our cohort. Notably, three patients post-hot maintained high post-SVR expression of type I IFNs (IFNAR1/2, IRF4), type III IFNs (IFNL1-2), and a mixed inflammatory and anti-inflammatory/profibrotic gene signature (TLRs, NF $\kappa$ B, TNF, TGF $\beta$ , IL4/IL13, IL10) (Figures 4B-E, 5). Although post-hot patients clustered with the pre-hot patients, their gene expression profile was distinct from both pre-hot and post-cold patients, and, since this pattern was observed in only a small subgroup, this finding should be considered preliminary and hypothesis-generating.

T cell dynamics further contributed to pre- and post-treatment hepatic immune heterogeneity. Restoration of cytotoxic and exhausted CD8 T cells after HCV treatment has been documented (Martin et al., 2014; Osuch et al., 2020), whereas some systemic populations, such as mucosal-associated invariant T cells (MAIT), remain dysfunctional (Hengst et al., 2016). In the gene expression subset, *CD4* expression was reduced in chronic HCV and did not significantly recover post-SVR, likely due to T cell exhaustion. HIV coinfection did not significantly impact *CD4* expression in coinfected patients post-DAA treatment (Supplementary Figure S5). *CD8A* gene expression, a marker of cytotoxic CD8+ T cells, increased with chronic HCV but remain unchanged post-treatment. Individual variability, however, reduced the statistical significance of the findings (Figure 3D) (BroChado-Kith et al., 2021; Medrano et al., 2021).

Despite normal transaminases, persistent portal inflammation was seen in 14 out of 17 patients post-DAA (82.3%, 95%CI: 64.2% - 100%) (Table 1). Some studies have reported that about 10% of the patients with ongoing inflammation will still have mildly abnormal liver enzymes after treatment (Welsch et al., 2017).

In parallel, spectral imaging of a separate subset revealed heterogeneity in hepatic T cell populations. Inter-patient variability was a major factor contributing to the lack of statistical significance when comparing groups, highlighting the importance of considering patient-level differences in this analysis and the partial overlap with the gene expression cohort. Prior work linked CD3+CD45RO+memory T cells with fibrosis progression in metabolic dysfunction-associated steatotic liver disease/metabolic dysfunction-associated steatohepatitis (MASLD/MASH) (Sanchez et al., 2023), suggesting a role in HCV-related liver disease. Memory T cells (CD45RO+), indicative of antigen-experienced T cells adapting to persistent infection, contributed to this heterogeneity (Figure 7). Memory T

cells inhibit NLRP3 activation (Beynon et al., 2012), which was upregulated in the pre-hot group (Supplementary Table S8).

By analyzing clinical data, histopathology, and gene expression data, we observed a significant positive association between the prehot profile and adverse outcomes (OR = 14.0, 95% CI: 1.31-178.5; p = 0.049) (Figures 8A, C). However, this association was no longer significant after adjusting for baseline fibrosis stage, MHAI, and HIV status (p = 0.328). Baseline MHAI scores (OR = 1.90, 95% CI: 0.72-6.34) and fibrosis stage (OR = 1.65, 95% CI: 0.44-9.97) showed trends toward predicting poor outcomes, but neither reached statistical significance. These findings suggest that greater baseline inflammation and fibrosis may contribute to post-treatment risk, though larger studies are needed to confirm these associations (Mendizabal et al., 2020). The wide confidence intervals for all predictors, including pre-cold and pre-hot profiles (95% CI: 0.18-2123), suggest the lack of statistical significance is not necessarily an absence of biological relationships. Six patients (27.2%) had advanced fibrosis/cirrhosis, two of whom developed end-stage liver disease (ESLD) (pt 14, 20). Three patients (13.6%) died from liver cancer (pt 4 and 19: HCC, pt 10: ChCA), consistent with reports of a 60-70% reduction in liver-related mortality after achieving SVR (Dang et al., 2020) (Table 1). Genes upregulated in pre-hot patients (CXCR4, BCL2, FYN) (Figure 4A) were associated with liver cancer progression, aligning with previous studies (Lin et al., 2014; Hosseini-Khah et al., 2021; Huang et al., 2022), while viral load showed no correlation (data not shown).

A key strength of this study is the use of paired liver biopsies pre- and post-DAA, enabling direct assessment of histopathology, gene and protein changes, and patient-specific immune responses. Analyses accounted for potential confounding comorbidities (fibrosis stage, MHAI, and HIV status). However, the cohort was relatively small, assays were performed on non-overlapping sample subsets, and some tissue was sufficient only for RNA extraction or spectral imaging. Despite these limitations, the dataset provides a unique and comprehensive view of hepatic immune dynamics, capturing meaningful biological variability among study patients. These findings should be viewed as exploratory and hypothesisgenerating, underscoring the need for larger studies to clarify whether pretreatment molecular signatures can provide prognostic information beyond established histologic markers.

DAA treatment effectively controlled infection, deactivated antiviral pathways, and reduced inflammation in most patients, despite initial variability in gene expression, MHAI scores, and fibrosis stages. This study is among the first to identify heterogeneous macrophage subsets in liver biopsies using multiplex immunofluorescence, aligning with recent single-cell findings. Memory T cells were commonly observed before DAA treatment and in some patients with persistent inflammation following treatment. Despite achieving SVR and normalization of gene expression patterns, patients with elevated baseline inflammation and fibrosis, features that overlap with the molecularly defined pre-hot signature, remain at risk for adverse outcomes following DAA treatment. This underscores the need for advanced risk stratification tools, ideally through future studies that

integrate gene and protein expression data with clinical parameters. Until molecular profiling becomes clinically accessible, closer monitoring of such patients can be guided by standard tools. By enabling precise, personalized monitoring, this approach has the potential to revolutionize patient management and significantly improve outcomes for high-risk individuals.

# Data availability statement

All data generated or analyzed in this study are included in the article and its Supplementary Materials. Additional information is available from the corresponding author(s) upon request.

# **Ethics statement**

The studies involving humans were approved by The University of Texas Medical Branch (UTMB) Institutional Review Board (IRB#13-0511). The studies were conducted in accordance with the local legislation and institutional requirements. The participants provided their written informed consent to participate in this study.

## **Author contributions**

DM: Data curation, Formal Analysis, Methodology, Writing – original draft. EA: Data curation, Formal Analysis, Methodology, Validation, Writing – original draft, Writing – review & editing. TW: Formal Analysis, Software, Writing – review & editing. SK: Formal Analysis, Software, Writing – review & editing. DB: Software, Writing – review & editing. JZ: Data curation, Writing – review & editing. AR: Formal Analysis, Software, Writing – review & editing. MF: Resources, Writing – review & editing. VC: Writing – review & editing. KH: Formal Analysis, Methodology, Visualization, Writing – review & editing. HS: Conceptualization, Formal Analysis, Project administration, Supervision, Writing – review & editing. OS: Data curation, Formal Analysis, Methodology, Validation, Writing – original draft, Writing – review & editing.

# **Funding**

The author(s) declare financial support was received for the research and/or publication of this article. The authors gratefully acknowledge the financial support provided by their grant funding sources. OS, EA, SK, HS, DB, AR, and HLS were partially supported by an R01 from NIDDK (1R01DK125730-01A1-4). OS and HSL were additionally supported by a Moody Endowment Grant (2014-07; LIME 19016). Preliminary optimization studies were partly supported by the National Center for Advancing Translational Science Clinical and Translational Science Awards Grant NCATS CTSA Grant KL2 Scholars Program (KL2TR001441-06). The

acquisition of the Vectra 3 microscope was made possible through funding from the UT System Faculty Science and Technology Acquisition and Retention (STARs) Program. AR and SK were supported by CCSG Bioinformatics Shared Resource 5 P30 CA046592, a gift from Agilent Technologies, and a Precision Health Investigator award from U-M Precision Health. The NCI Grant R37-CA214955 partially supported SK and AR. SK and AR were also partially supported by the University of Michigan (U-M) startup institutional research funds. SK and AR were also supported by a Research Scholar Grant from the American Cancer Society (RSG-16-005-01).

# Acknowledgments

We would like to thank Dr. Netanya Utay, MD, for initiating this study. We extend our sincere gratitude to Jeffrey East, PA, for his assistance in obtaining patient consent. We also thank Min Zhang, licensed histology technician, for cutting the liver biopsy tissue blocks and assisting with troubleshooting.

## Conflict of interest

HSL and OS have a filed patent titled "Systems and methods for spectral imaging characterization of macrophages for use in personalization of targeted therapies to prevent fibrosis development in patients with chronic liver disease." Board of Regents, The University of Texas System, United States, Galveston, Texas; Pub. No: US 20210293814. AR serves as a member of Voxel Analytics LLC and consults for Tempus Labs Inc. and Tata Consultancy Services Ltd.

The remaining authors declare that the research was conducted in the absence of any commercial or financial relationships that could be construed as a potential conflict of interest.

# Generative AI statement

The author(s) declare that no Generative AI was used in the creation of this manuscript.

Any alternative text (alt text) provided alongside figures in this article has been generated by Frontiers with the support of artificial intelligence and reasonable efforts have been made to ensure accuracy, including review by the authors wherever possible. If you identify any issues, please contact us.

# Publisher's note

All claims expressed in this article are solely those of the authors and do not necessarily represent those of their affiliated organizations, or those of the publisher, the editors and the reviewers. Any product that may be evaluated in this article, or claim that may be made by its manufacturer, is not guaranteed or endorsed by the publisher.

# Supplementary material

The Supplementary Material for this article can be found online at: https://www.frontiersin.org/articles/10.3389/fcimb.2025. 1662184/full#supplementary-material

#### SUPPLEMENTARY FIGURE 1

CIBERSORT was used to estimate the abundance of cell populations, including macrophages, T cells, B cells, and NK cells, using genes from the PanCancer Immune Panel. The key genes contributing to the prediction and deconvolution of these populations are shown: (A) genes critical for cell deconvolution before and after DAA treatment, and (B) genes relevant within subclusters (pre-hot, pre-cold, post-hot, post-cold, and controls). Heatmaps were generated using each group's average Z-score values (range:  $\pm$  2), with red indicating high gene expression and blue representing low gene expression.

#### SUPPLEMENTARY FIGURE 2

Comparison of clinical data from patients pre- and post-DAA treatment subclustered by gene expression patterns. We compared the clinical and laboratory data in patients pre- and post-DAA therapy with two distinct patterns of gene expression and clustering: Pre-hot (high gene expression profile pre-DAA therapy compared to controls), pre-cold (low gene expression profile pre-DAA therapy compared to controls), post-hot (high gene expression post-DAA therapy comparable to pre-hot), and post-cold (low gene expression post-DAA therapy comparable to controls). The prehot subcluster showed an increased MHAI score, ALT, and AST, which decreased post-DAA treatment. Liver biopsies were graded for inflammatory activity using the MHAI scoring criteria (0-18) and staged for fibrosis using the Ishak (1-6) criteria (Ishak et al., 1995). Histological and laboratory data were analyzed using limma (R/Bioconductor), accounting for paired and unpaired samples with duplicateCorrelation function; linear models with empirical Bayes moderation were used, and p-values were adjusted by the B-H FDR method. pre, (pre-DAA treatment); post, (post-DAA treatment); MHAI, modified hepatitis activity index; ALT, Alanine transaminase; AST, Aspartate aminotransferase; ALP, Alkaline phosphatase; FFPE, Formalin-fixed paraffin-embedded; PT, Prothrombin time; INR, International Normalized Ratio.

#### SUPPLEMENTARY FIGURE 3

(A-F) Volcano plots illustrate differentially expressed genes in patients before and after DAA treatment. Volcano plots show log2 fold change versus –log10

adjusted p-value (Benjamini-Yekutieli). Horizontal dashed lines indicating – log10 B-Y adjusted p < 0.05 and vertical dashed lines representing log2 fold change < -0.6 or > 0.6. Red dots denote statistically significantly differentially expressed mRNAs. Abbreviations: Ctrls (controls), pre-hot (high gene expression profile pre-DAA therapy), pre-cold (low gene expression profile pre-DAA therapy), post-hot (high gene expression post-DAA therapy), and post-cold (low gene expression post-DAA therapy).

#### SUPPLEMENTARY FIGURE 4

(A-E) The Venn diagram illustrates genes significantly expressed across preand post-DAA therapy subcluster groups (pre-hot, pre-cold, and post-hot) compared to the control group. The post-cold subcluster group was excluded due to the absence of significantly expressed genes relative to the control. Genes were selected based on an adjusted Benjamini-Yekutieli (B-Y) p-value < 0.05 and a log2-fold change < -0.6 or > 0.6. Genes in red represent upregulated expression, while those in blue indicate downregulated expression. Pre-hot, high gene expression profile pre-DAA therapy; pre-cold, low gene expression profile pre-DAA therapy; post-hot, high gene expression post-DAA therapy.

#### SUPPLEMENTARY FIGURE 5

Gene expression patterns in patients with HCV were not significantly affected by their HIV status. (A) Box plots comparing the gene expression of CD4, CD8A, and FoxP3 before and after DAA treatment revealed no significant differences between HIV-coinfected and non-coinfected patients. (B, C) To determine whether HIV coinfection was a confounding factor in the observed gene expression differences before and after treatment, we conducted a PCA (B) and a Fisher's exact test analysis (C) on groups of patients with HCV pre-(pre-hot, n = 9; pre-cold, n = 8) and post- (post-hot, n = 3; post-cold, n = 11) treatment. PCA demonstrated overlapping clustering between HIVcoinfected and non-coinfected patients, both pre- and post-treatment, with clustering influenced primarily by "hot" or "cold" status, as previously described. Fisher's exact test further confirmed that HIV status did not significantly associate with gene expression patterns pre- or posttreatment (p > 0.05). Normal distribution (Shapiro-Wilk) was assessed, and an unpaired one-way ANOVA or Mann-Whitney test was used to compare the differences between the groups. \*p < 0.05; \*\*p < 0.01; \*\*\*p < 0.001. PCA of log2-transformed data was used for clustering analysis. The Fisher test assessed gene expression-outcome association (OR >1 = positive association). Ctrl, controls; pre-DAA HIV+, pre-DAA treatment coinfected with HIV; pre-DAA HIV-, pre-DAA treatment without coinfection with HIV; post-DAA HIV+, post-DAA treatment coinfected with HIV; post-DAA HIV-, post-DAA treatment without coinfection with HIV.

# References

Abutaleb, A., and Sherman, K. E. (2018). A changing paradigm: management and treatment of the HCV/HIV-co-infected patient. *Hepatol. Int.* 12, 500–509. doi: 10.1007/s12072-018-9896-4

Ahmed, F., Ibrahim, A., Cooper, C. L., Kumar, A., and Crawley, A. M. (2019). Chronic hepatitis C virus infection impairs M1 macrophage differentiation and contributes to CD8. *Cells* 8(4), 374–392. doi: 10.3390/cells8040374

Barili, V., Fisicaro, P., Montanini, B., Acerbi, G., Filippi, A., Forleo, G., et al. (2020). Targeting p53 and histone methyltransferases restores exhausted CD8+ T cells in HCV infection. *Nat. Commun.* 11, 604. doi: 10.1038/s41467-019-14137-7

Beynon, V., Quintana, F. J., and Weiner, H. L. (2012). Activated human CD4 +CD45RO+ memory T-cells indirectly inhibit NLRP3 inflammasome activation through downregulation of P2X7R signalling. *PLoS One* 7, e39576. doi: 10.1371/journal.pone.0039576

Bhattacharya, D., Aronsohn, A., Price, J., Lo Re, V., and Panel, A-IHG. (2023). Hepatitis C guidance 2023 update: AASLD-IDSA recommendations for testing, managing, and treating hepatitis C virus infection. *Clin. Infect. Dis.* 1-18, ciad319. doi: 10.1093/cid/ciad319

Bility, M. T., Nio, K., Li, F., McGivern, D. R., Lemon, S. M., Feeney, E. R., et al. (2016). Chronic hepatitis C infection-induced liver fibrogenesis is associated with M2 macrophage activation. *Sci. Rep.* 6, 39520. doi: 10.1038/srep39520

Boldanova, T., Suslov, A., Heim, M. H., and Necsulea, A. (2017). Transcriptional response to hepatitis C virus infection and interferon-alpha treatment in the human liver. *EMBO Mol. Med.* 9, 816–834. doi: 10.15252/emmm.201607006

Brochado-Kith, Ó., Martínez, I., Berenguer, J., González-García, J., Salgüero, S., Sepúlveda-Crespo, D., et al. (2021). HCV cure with direct-acting antivirals improves

liver and immunological markers in HIV/HCV-coinfected patients. Front. Immunol. 12. doi: 10.3389/fimmu.2021.723196

Burchill, M. A., Salomon, M. P., Golden-Mason, L., Wieland, A., Maretti-Mira, A. C., Gale, M., et al. (2021). Single-cell transcriptomic analyses of T cells in chronic HCV-infected patients dominated by DAA-induced interferon signaling changes. *PLoS Pathog.* 17, e1009799. doi: 10.1371/journal.ppat.1009799

Burki, T. (2024). WHO's 2024 global hepatitis report. Lancet Infect. Dis. 24, e362–e363. doi: 10.1016/\$1473-3099(24)00307-4

Chen, B., Khodadoust, M. S., Liu, C. L., Newman, A. M., and Alizadeh, A. A. (2018). Profiling tumor infiltrating immune cells with CIBERSORT. *Methods Mol. Biol.* 1711, 243–259. doi: 10.1007/978-1-4939-7493-1\_12

Corbeau, P., and Reynes, J. (2011). Immune reconstitution under antiretroviral therapy: the new challenge in HIV-1 infection. Blood 117, 5582–5590. doi: 10.1182/blood-2010-12-322453

Cui, A., Li, B., Wallace, M. S., Gonye, A. L. K., Oetheimer, C., Patel, H., et al. (2024). Single-cell atlas of the liver myeloid compartment before and after cure of chronic viral hepatitis. *J. Hepatol.* 80, 251–267. doi: 10.1016/j.jhep.2023.02.040

D'Ambrosio, R., Aghemo, A., Rumi, M. G., Ronchi, G., Donato, M. F., Paradis, V., et al. (2012). A morphometric and immunohistochemical study to assess the benefit of a sustained virological response in hepatitis C virus patients with cirrhosis. *Hepatology* 56, 532–543. doi: 10.1002/hep.25606

Dang, H., Yeo, Y. H., Yasuda, S., Huang, C. F., Iio, E., Landis, C., et al. (2020). Cure with interferon-free direct-acting antiviral is associated with increased survival in

patients with hepatitis C virus-related hepatocellular carcinoma from both east and west. *Hepatology* 71, 1910–1922. doi: 10.1002/hep.30988

Fattovich, G., Stroffolini, T., Zagni, I., and Donato, F. (2004). Hepatocellular carcinoma in cirrhosis: incidence and risk factors. *Gastroenterology* 127, S35–S50. doi: 10.1053/j.gastro.2004.09.014

Gazzola, L., Tincati, C., Bellistri, G. M., Monforte, A., and Marchetti, G. (2009). The absence of CD4+ T cell count recovery despite receipt of virologically suppressive highly active antiretroviral therapy: clinical risk, immunological gaps, and therapeutic options. *Clin. Infect. Dis.* 48, 328–337. doi: 10.1086/595851

Hengst, J., Strunz, B., Deterding, K., Ljunggren, H. G., Leeansyah, E., Manns, M. P., et al. (2016). Nonreversible MAIT cell-dysfunction in chronic hepatitis C virus infection despite successful interferon-free therapy. *Eur. J. Immunol.* 46, 2204–2210. doi: 10.1002/eji.201646447

Holmes, J. A., Carlton-Smith, C., Kim, A. Y., Dumas, E. O., Brown, J., Gustafson, J. L., et al. (2019). Dynamic changes in innate immune responses during direct-acting antiviral therapy for HCV infection. *J. Viral Hepat.* 26, 362–372. doi: 10.1111/jvh.13041

Hosseini-Khah, Z., Babaei, M. R., Tehrani, M., Cucchiarini, M., Madry, H., Ajami, A., et al. (2021). SOX2 and bcl-2 as a novel prognostic value in hepatocellular carcinoma progression. *Curr. Oncol.* 28, 3015–3029. doi: 10.3390/curroncol28040264

Hou, J., van Oord, G., Groothuismink, Z. M., Claassen, M. A., Kreefft, K., Zaaraoui-Boutahar, F., et al. (2014). Gene expression profiling to predict and assess the consequences of therapy-induced virus eradication in chronic hepatitis C virus infection. *J. Virol.* 88, 12254–12264. doi: 10.1128/JVI.00775-14

Hsieh, Y. C., Lee, K. C., Su, C. W., Lan, K. H., Huo, T. I., Wang, Y. J., et al. (2021). Persistent liver inflammation in chronic hepatitis C patients with advanced fibrosis after direct-acting antivirals induced sustained virological response. *J. Chin. Med. Assoc.* 84, 472–477. doi: 10.1097/JCMA.0000000000000517

Huang, C., Zhou, J., Nie, Y., Guo, G., Wang, A., and Zhu, X. (2022). A new finding in the key prognosis-related proto-oncogene FYN in hepatocellular carcinoma based on the WGCNA hub-gene screening trategy. *BMC Cancer.* 22, 380. doi: 10.1186/s12885-022-09388-5

Ishak, K., Baptista, A., Bianchi, L., Callea, F., De Groote, J., Gudat, F., et al. (1995). Histological grading and staging of chronic hepatitis. *J. Hepatol.* 22, 696–699. doi: 10.1016/0168-8278(95)80226-6

Ko, J. Y., Haight, S. C., Schillie, S. F., Bohm, M. K., and Dietz, P. M. (2019). National trends in hepatitis C infection by opioid use disorder status among pregnant women at delivery hospitalization - United States, 2000-2015. MMWR Morb Mortal Wkly Rep. 68, 833–838. doi: 10.15585/mmwr.mm6839a1

Lin, L., Han, M. M., Wang, F., Xu, L. L., Yu, H. X., and Yang, P. Y. (2014). CXCR7 stimulates MAPK signaling to regulate hepatocellular carcinoma progression. *Cell Death Dis.* 5, e1488. doi: 10.1038/cddis.2014.392

Listopad, S., Magnan, C., Asghar, A., Stolz, A., Tayek, J. A., Liu, Z. X., et al. (2022). Differentiating between liver diseases by applying multiclass machine learning approaches to transcriptomics of liver tissue or blood-based samples. *JHEP Rep.* 4, 100560. doi: 10.1016/j.jhepr.2022.100560

MacParland, S. A., Liu, J. C., Ma, X. Z., Innes, B. T., Bartczak, A. M., Gage, B. K., et al. (2018). Single cell RNA sequencing of human liver reveals distinct intrahepatic macrophage populations. *Nat. Commun.* 9, 4383. doi: 10.1038/s41467-018-06318-7

Martin, B., Hennecke, N., Lohmann, V., Kayser, A., Neumann-Haefelin, C., Kukolj, G., et al. (2014). Restoration of HCV-specific CD8+ T cell function by interferon-free therapy. *J. Hepatol.* 61, 538–543. doi: 10.1016/j.jhep.2014.05.043

Medrano, L. M., Berenguer, J., Salgüero, S., González-García, J., Díez, C., Hontañón, V., et al. (2021). Successful HCV therapy reduces liver disease severity and inflammation biomarkers in HIV/HCV-coinfected patients with advanced cirrhosis: A cohort study. Front. Med. (Lausanne). 8. doi: 10.3389/fmed.2021.615342

Mendizabal, M., Piñero, F., Ridruejo, E., Herz Wolff, F., Anders, M., Reggiardo, V., et al. (2020). Disease progression in patients with hepatitis C virus infection treated with direct-acting antiviral agents. *Clin. Gastroenterol. Hepatol.* 18, 2554–2563.e3. doi: 10.1016/j.cgh.2020.02.044

Noureddin, M., Rotman, Y., Zhang, F., Park, H., Rehermann, B., Thomas, E., et al. (2015). Hepatic expression levels of interferons and interferon-stimulated genes in patients with chronic hepatitis C: A phenotype-genotype correlation study. *Genes Immun.* 16, 321–329. doi: 10.1038/gene.2015.11

Oru, E., Trickey, A., Shirali, R., Kanters, S., and Easterbrook, P. (2021). Decentralisation, integration, and task-shifting in hepatitis C virus infection testing and treatment: a global systematic review and meta-analysis. *Lancet Glob Health* 9, e431–e445. doi: 10.1016/S2214-109X(20)30505-2

Osuch, S., Laskus, T., Berak, H., Perlejewski, K., Metzner, K. J., Paciorek, M., et al. (2020). Decrease of T-cells exhaustion markers programmed cell death-1 and T-cell immunoglobulin and mucin domain-containing protein 3 and plasma IL-10 levels after successful treatment of chronic hepatitis C. Sci. Rep. 10, 16060. doi: 10.1038/s41598-020-73137-6

Poynard, T., Bedossa, P., and Opolon, P. (1997). Natural history of liver fibrosis progression in patients with chronic hepatitis C. The OBSVIRC, METAVIR, CLINIVIR, and DOSVIRC groups. *Lancet* 349, 825–832. doi: 10.1016/s0140-6736 (96)07642-8

Putra, J., Schiano, T. D., and Fiel, M. I. (2018). Histological assessment of the liver explant in transplanted hepatitis C virus patients achieving sustained virological response with direct-acting antiviral agents. *Histopathology* 72, 990–996. doi: 10.1111/his.13453

Saha, B., Kodys, K., and Szabo, G. (2016). Hepatitis C virus-induced monocyte differentiation into polarized M2 macrophages promotes stellate cell activation via TGF- $\beta$ . Cell Mol. Gastroenterol. Hepatol. 2, 302–316.e8. doi: 10.1016/j.jcmgh.2015.12.005

Saldarriaga, O. A., Dye, B., Pham, J., Wanninger, T. J., and Kueht, M. D. (2021). Comparison of liver biopsies before and after direct-acting antiviral therapy for hepatitis C and correlation with clinical outcome. *Sci. Rep.* 11, 14506. doi: 10.1038/s41598-021-93881-7

Saldarriaga, O. A., Freiberg, B., Krishnan, S., Rao, A., Burks, J., Booth, A. L., et al. (2020). Multispectral imaging enables characterization of intrahepatic macrophages in patients with chronic liver disease. *Hepatol. Commun.* 4, 708–723. doi: 10.1002/hep4.1494

Saldarriaga, O. A., Wanninger, T. G., Arroyave, E., Gosnell, J., Krishnan, S., Oneka, M., et al. (2024). Heterogeneity in intrahepatic macrophage populations and druggable target expression in patients with steatotic liver disease-related fibrosis. *JHEP Rep.* 6, 100958. doi: 10.1016/j.jhepr.2023.100958

Salum, G. M., Dawood, R. M., Abd El-Meguid, M., Ibrahim, N. E., Abdel Aziz, A. O., and El Awady, M. K. (2020). Correlation between IL28B/TLR4 genetic variants and HCC development with/without DAAs treatment in chronic HCV patients. *Genes Dis.* 7, 392–400. doi: 10.1016/j.gendis.2019.05.004

Sanchez, J. I., Parra, E. R., Jiao, J., Solis Soto, L. M., Ledesma, D. A., Saldarriaga, O. A., et al. (2023). Cellular and molecular mechanisms of liver fibrosis in patients with NAFLD. *Cancers (Basel)*. 15(11), 2871–2886. doi: 10.3390/cancers15112871

Terczyńska-Dyla, E., Bibert, S., Duong, F. H., Krol, I., Jørgensen, S., Collinet, E., et al. (2014). Reduced IFNλ4 activity is associated with improved HCV clearance and reduced expression of interferon-stimulated genes. *Nat. Commun.* 5, 5699. doi: 10.1038/ncomms6699

Tu, Z., Pierce, R. H., Kurtis, J., Kuroki, Y., Crispe, I. N., and Orloff, M. S. (2010). Hepatitis C virus core protein subverts the antiviral activities of human Kupffer cells. *Gastroenterology* 138, 305–314. doi: 10.1053/j.gastro.2009.09.009

Vranjkovic, A., Deonarine, F., Kaka, S., Angel, J. B., Cooper, C. L., and Crawley, A. M. (2019). Direct-acting antiviral treatment of HCV infection does not resolve the dysfunction of circulating CD8. *Front. Immunol.* 10. doi: 10.3389/fimmu.2019.01926

Welsch, C., Efinger, M., von Wagner, M., Herrmann, E., Zeuzem, S., Welzel, T. M., et al. (2017). Ongoing liver inflammation in patients with chronic hepatitis C and sustained virological response. *PLoS One* 12, e0171755. doi: 10.1371/journal.pone.0171755

Whitcomb, E., Choi, W. T., Jerome, K. R., Cook, L., Landis, C., Ahn, J., et al. (2017). Biopsy specimens from allograft liver contain histologic features of hepatitis C virus infection after virus eradication. *Clin. Gastroenterol. Hepatol.* 15, 1279–1285. doi: 10.1016/j.cgh.2017.04.041

Young, J., Psichogiou, M., Meyer, L., Ayayi, S., Grabar, S., Raffi, F., et al. (2012). CD4 cell count and the risk of AIDS or death in HIV-Infected adults on combination antiretroviral therapy with a suppressed viral load: a longitudinal cohort study from COHERE. *PLoS Med.* 9, e1001194. doi: 10.1371/journal.pmed.1001194

Zhao, S., Si, M., Deng, X., Wang, D., Kong, L., and Zhang, Q. (2022). HCV inhibits M2a, M2b and M2c macrophage polarization *via* HCV core protein engagement with Toll-like receptor 2. *Exp. Ther. Med.* 24, 522. doi: 10.3892/etm.2022.11448

# Glossary

AI	AI-artificial intelligence	JAK	Janus kinase
ALP	alkaline phosphatase	MAIT	mucosal-associated invariant T cells
ALT	alanine aminotransferase	MASLD	metabolic dysfunction-associated steatotic liver disease
ANOVA	Analysis of Variance	MASH	metabolic dysfunction-associated steatohepatitis
AST	aspartate aminotransferase	MCL	Markov cluster algorithm
BMI	body mass index	MHAI	modified hepatitis activity index
В-Н	Benjamini-Hochberg	MHC	major histocompatibility complex
B-Y	Benjamini-Yekutieli	MX	myxovirus resistance
CAP	College of American Pathologists	NKC	natural killer cells
ChCA CLIA	cholangiocarcinoma	NLRP	nucleotide-binding domain, leucine-rich-containing family, pyrin domain containing protein
DAA	Clinical Laboratory Improvement Amendments	PCA	principal component analysis
DAA	direct-acting antiviral	POST	post-DAA treatment
DEG	4',6-diamidino-2-phenylindole differentially expressed genes	PRE	pre-DAA treatment
ESLD	end-stage liver disease	Pt	patient
FDR	false discovery rate	PT	prothrombin time
FFPE	formalin-fixed, paraffin-embedded	RCC	resource compiler files
H&E	hematoxylin and eosin	RNA	ribonucleic acid
HAART	highly active antiretroviral therapy	ROIs	regions of interest
HCC	hepatocellular carcinoma	STAT	signal transducer and activation of transcription
HCV	hepatitis C virus	STRING	search tool for the retrieval of interacting genes/proteins
HIV	human immunodeficiency virus	SVR	sustained virologic response
IFI	interferon-inducible protein	TGFB	transforming growth factor beta
IFN	interferon	TIFF	tagged image file format
INR	international normalized ratio	TNF	tumor necrosis factor
IRB	Institutional Review Board	t-SNE	t-distributed stochastic neighbor embedding
ISG	interferon-stimulated genes	UTMB	University of Texas Medical Branch